DUDLEY KNOX LIBRARY
NAVAL POSTGRADUATE SCHOOL
MONTEREY CA 93940

NPS 67-80-017

NAVAL POSTGRADUATE SCHOOL
Monterey, California

THESIS

ANALYSIS AND WIND TUNNEL TESTS OF A STATIC PRESSURE PROBE USED TO SENSE ALTITUDE THROUGH MEASUREMENT OF STATIC PRESSURE

by

Kenneth Delmer Tillotson

December, 1980

Thesis Advisor: A. E. Fuhs

Approved for public release; distribution unlimited

Prepared for: Mr. Ronald Dettling
Naval Weapons Center
China Lake, CA 93555

T197859

NAVAL POSTGRADUATE SCHOOL
Monterey, California

Rear Admiral J. J. Ekelund Superintendent	David Schrady Acting Provost

This thesis prepared in conjunction with research supported in part by the Naval Weapons Center, China Lake, California.

Reproduction of all or part of this report is authorized.

Released as a
Technical Report by:

DUDLEY KNOX LIBRARY

REPORT DOCUMENTATION PAGE

READ INSTRUCTIONS
BEFORE COMPLETING FORM

1. REPORT NUMBER NPS 67-80-017	2. GOVT ACCESSION NO.	3. RECIPIENT'S CATALOG NUMBER
4. TITLE (and Subtitle) Analysis and Wind Tunnel Tests of a Static Pressure Probe Used to Sense Altitude Through Measurement of Static Pressure		5. TYPE OF REPORT & PERIOD COVERED Master's Thesis December, 1980
		6. PERFORMING ORG. REPORT NUMBER
7. AUTHOR(s) Kenneth Delmer Tillotson		8. CONTRACT OR GRANT NUMBER(s)
9. PERFORMING ORGANIZATION NAME AND ADDRESS Naval Postgraduate School Monterey, California 93940		10. PROGRAM ELEMENT, PROJECT, TASK AREA & WORK UNIT NUMBERS
11. CONTROLLING OFFICE NAME AND ADDRESS Naval Postgraduate School Monterey, California 93940		12. REPORT DATE December, 1980
		13. NUMBER OF PAGES 78
14. MONITORING AGENCY NAME & ADDRESS(if different from Controlling Office) Mr. Ronald Dettling Naval Weapons Center China Lake, California 93555		15. SECURITY CLASS. (of this report) UNCLASSIFIED
		15a. DECLASSIFICATION/DOWNGRADING SCHEDULE

16. DISTRIBUTION STATEMENT (of this Report)

Approved for public release; distribution unlimited

17. DISTRIBUTION STATEMENT (of the abstract entered in Block 20, if different from Report)

18. SUPPLEMENTARY NOTES

19. KEY WORDS (Continue on reverse side if necessary and identify by block number)

AEROSPIKE
STATIC PRESSURE PROBE

20. ABSTRACT (Continue on reverse side if necessary and identify by block number)

A static pressure probe was tested to determine the feasibility of using the probe, as an integral part of a missile nose, to sense missile altitude. Experiments were conducted at Mach 2.0 and at Mach 1.51.

At Mach 2.0, the static pressure probe will perform within altitude specifications of 25,000 feet ± 2,000 feet at angles of attack ranging

20. (cot'd.)

from - 8 to + 8 degrees. At Mach 2.0, within an angle-of-attack ranging from 0 to 6 degrees, the probe will measure free stream static pressure within 4 percent; a 4 percent error in measurement is equivalent to an altitude error of 900 feet. The missile nose shock will remain downstream of the probe pressure ports for flight Mach numbers above 1.5.

Approved for public release; distribution unlimited

Analysis and Wind Tunnel Tests of a Static Pressure Probe Used to Sense Altitude Through Measurement of Static Pressure

by

Kenneth Delmer Tillotson
Lieutenant Commander, United States Navy
B.S., United States Naval Academy, 1968

Submitted in partial fulfillment of the
requirements for the degree of

MASTER OF SCIENCE IN ENGINEERING SCIENCE

from the

NAVAL POSTGRADUATE SCHOOL
December, 1980

Thesis
T485
c.1

ABSTRACT

A static pressure probe was tested to determine the feasibility of using the probe, as an integral part of a missile nose, to sense missile altitude. Experiments were conducted at Mach 2.0 and at Mach 1.51.

At Mach 2.0, the static pressure probe will perform within altitude specifications of 25,000 feet ± 2,000 feet at angles of attack ranging from - 8 to + 8 degrees. At Mach 2.0, within an angle-of-attack ranging from 0 to 6 degrees, the probe will measure free stream static pressure within 4 percent; a 4 percent error in measurement is equivalent to an altitude error of 900 feet. The missile nose shock will remain downstream of the probe pressure ports for flight Mach numbers above 1.5.

TABLE OF CONTENTS

I. INTRODUCTION 12

A. BACKGROUND 12

B. THESIS PURPOSE 14

II. THEORY 15

A. STATIC PRESSURE PROBE DESIGN 15

B. STATIC PRESSURE DISTRIBUTION 17

C. RESULTS OF THEORETICAL CALCULATIONS 17

1. Theoretical Calculations 17

2. Probe Pressure Hole Location 18

3. Error in Altitude Due to Error in Pressure Measurement 18

4. Probe Pressure Readings at Angle-of-Attack 19

III. EXPERIMENTAL APPARATUS 22

A. WIND TUNNEL 22

1. Mach 2.0 Wind Tunnel Tests 22

2. Mach 1.4 Wind Tunnel Tests 23

3. Mach 1.51 Wind Tunnel Tests 23

B. MODEL DESIGN 24

C. INSTRUMENTATION 26

IV. EXPERIMENTAL RESULTS 27

A. MACH 2.0 EXPERIMENTAL RESULTS 27

1. Data Reduction Technique 27

2. Static Pressure Probe Performance 28

B. MACH 1.51 EXPERIMENTAL RESULTS 29

V. CONCLUSIONS AND RECOMMENDATIONS 33

A. CONCLUSIONS 33

B. RECOMMENDATIONS 33

FIGURES 35

APPENDIX A: PRESSURE DISTRIBUTION PROGRAM LISTING AND SAMPLE DATA RUNS 62

APPENDIX B: COMPUTER PROGRAM AND SAMPLE DATA RUN FOR CALCULATING PROBE PLENUM PRESSURE. 71

APPENDIX C: SEQUENTIAL LISTING OF TESTING. 73

LIST OF REFERENCES. 77

INITIAL DISTRIBUTION LIST 78

LIST OF FIGURES

1-1 Static Pressure Probe Interior to Missile Nose 35

1-2 Static Pressure Probe Both Extended and Interior to the Missile Nose. 36

2-1 General Static Pressure Probe Design 37

2-2 Shock Angle Versus Mach Number for Various Cone Angles 38

2-3 Theoretical Static Pressure Distribution as a Function of X/R_n for $M_\infty = 2.5$, $\beta = 10$ Degrees, and $\omega = 3$ Degrees. 39

2-4 Experimental Results of Static Pressure Probe at Angle-of-Attack for $M_\infty = 2.5$, $\beta = 10$ Degrees, and $\omega = 3$ Degrees. . . . 40

2-5 Static Pressure Probe Design for $\beta = 10$ Degrees and $\omega = 3$ Degrees. 41

2-6 Theoretical Probe Static Pressure Distribution for $M_\infty = 2.5$, $\beta = 10$ Degrees, and $\omega = 3$ Degrees. 42

2-7 Theoretical Probe Static Pressure Distribution for $M_\infty = 1.4$, 1.6, 1.8, and 2.0 at Zero Angle-of-Attack. 43

2-8 Static Pressure Probe Cross Section. 44

2-9 Theoretical Probe Static Pressure Distribution as a Function of Angle-of-Attack (α) for $M_\infty = 2.0$ 45

3-1 Naval Postgraduate School Supersonic Wind Tunnel and Associated Instrumentation (Rear Quarter View) 46

3-2 Naval Postgraduate School Supersonic Wind Tunnel and Associated Instrumentation (Front View). 47

3-3 Schlieren Photograph of the Model Mounted in the Wind Tunnel; $\alpha = 0$ Degrees and $M_\infty = 1.92$ 48

3-4 Theoretical Mach Number Gradient and the Shock Waves in the Wind Tunnel Test Section That Result from Using the Combination of Mach 1.4 (Bottom) and Mach 2.0 (Top) Nozzle Blocks. 49

3-5 Photograph of the Mach 2.0 and Mach 1.4 Nozzle Blocks Installed in the Wind Tunnel 50

3-6 Front View of the Model and Double-Wedge Airfoil Used to Mount the Model in the Wind Tunnel 51

3-7 Photograph of the Model Ogive Nose and the Extended Static Pressure Probe 52

3-8 Photograph of the Static Pressure Probe Mated to the Missile Nose. 53

3-9 Top View of the Model and Mounting Wedge 54

3-10 Photograph of the Model Mounted in the Wind Tunnel. 55

3-11 Close-Up View of the Model Mounted in the Wind Tunnel. 56

4-1 Plot of Experimental Results for $M_\infty = 1.92$: Angle-of-Attack Versus P/P_∞ and Probe Theoretical Performance. 57

4-2 Schlieren Photograph of the Model Oriented at $\alpha = +1$ Degree in the Wind Tunnel Operating at $M_\infty = 1.92$. 58

4-3 Schlieren Photograph of the Model in the Wind Tunnel Test Section: $M_\infty = 1.51$ and $\alpha = 4$ Degrees 59

4-4 Graph of Distance Versus Theoretical Mach Number and Pressure (PSIA) in the Wind Tunnel Test Section. 60

A-1 Schlieren Photograph of Shock in Wind Tunnel Test Section During an Attempt to Obtain Supersonic Flow with the Mach 1.4 Nozzle Blocks 61

LIST OF TABLES

2.1 Mathematically Possible Cases for Eq. 2-13 21

4.1 Sample Wind Tunnel Data: α = 0 Degrees and M_∞ = 1.92. 27

4.2 Sample Wind Tunnel Data: α = 2 Degrees and M_∞ = 1.92. 27

4.3 Angles-of-Attack Versus Theoretical and Experimental P/P_∞ for M_∞ = 2.0 28

4.4 Theoretical and Observed Pressure for a Combination of Mach 1.4 and Mach 2.0 Nozzle Blocks. 30

4.5 Sample Wind Tunnel Data: α = 4 Degrees and M_∞ = 1.92. 32

PARTIAL LIST OF SYMBOLS

α = Angle-of-Attack

β = Static Pressure Probe Conical Nose Half-Angle

M_∞ = Free Stream Mach Number

μ = Mach Angle

P = Static Pressure Measured by the Probe

P_∞ = Free Stream Static Pressure

ξ = 7.62 km

ρ = Density

ϕ = Probe Nose Shock Half-Angle

Re = Reynolds Number

R_n = Radius of the Probe Nose

x = Length of the Probe

y = Radius of the Probe

ω = Second Truncated Cone Half-Angle

ACKNOWLEDGEMENTS

The author wishes to express his most sincere gratitude and appreciation to Distinguished Professor Allen E. Fuhs of the Naval Postgraduate School for his guidance and help in the preparation and execution of this project. Funding support for this project was provided by the Naval Weapons Center, China Lake, California; Mr. Ron Dettling was the Project Monitor. Mr. S. Z. Pinckney, NASA, provided the probe design used in the project.

The author also would like to thank Lt. J. R. Schonberger, USN, for his help with the computer programs used in this research, his photographs, his talents, and his many hours of time and help during wind tunnel testing. In addition, I would like to thank my second reader, Professor T. H. Gawain, for his assistance and the theory used for a major portion of this research. Finally, I would like to thank my wife, Tish, for her help in the preparation of this report.

I. INTRODUCTION

A. BACKGROUND

The ZEPPO Rocket is an air-launched system designed to deliver an expendable pulse power communications jammer at long range. To achieve this objective, the system is loft-launched at angles up to 45 degrees and at high altitude. At the proper point in the trajectory, a deployment sequence is initiated by the fuze. At the end of this sequence, the expendable jammer is suspended and operated from a 17-foot diameter parachute with a descent rate of 10 to 12 feet per second. The ZEPPO system is 5 inches in diameter and 115 inches in length, and weighs approximately 135 pounds. The deployment system consists of: (1) a timer fuze in the nose; (2) an expulsion charge; (3) a drogue parachute; (4) a main parachute; and (5) an expendable electronic jammer.

The rocket motor is the production MK71 MOD 1 Zuni motor. The motor weighs 80 pounds, and is 73.3 inches in length and 5 inches in diameter. It has a thrust level of 6500 pounds force for 1.5 seconds, with a burnout spin rate of 30 to 33 revolutions per second.

The fuze, at the present time, is a modified MK375 MOD 0 timer fuze with a timing capability up to 140 seconds. It contains a black powder expulsion charge.

The drogue parachute has a cruciform geometry and is packed in a small bag that opens after motor separation. The main parachute is a lightweight 17-foot parachute adapted from the LUU-2/B flare system which is a standard production item. The chute is packed in a deployment sleeve

measuring 5 inches in diameter by eight feet in length; this sleeve drastically reduces snatch and opening loads, permitting the lightweight parachute to survive high "Q" deployment without damage.

The optimum point for deployment initiation is 25,000 feet, plus or minus 2,000 feet. Deployment at this altitude allows maximum payload time aloft, and therefore maximum operation time. System testing by the Naval Weapons Center, China Lake, California, has demonstrated that there is difficulty in attaining the optimum deployment altitude with the present fuzing system.

To remedy this situation, several alternatives were considered, one of which was a fuzing system initiated by a pressure-sensing switch, or Baro-Fuze. Two alternatives were considered for measuring pressure: a shock-swallowing air sensor and a static-pressure probe. The Naval Postgraduate School was selected to evaluate the effectiveness of the static-pressure probe. The probe selected for this evaluation was developed by Pinckney [1].

Figure 1-1 shows the probe interior to the missile nose, where it remains until after launch. After rocket motor burnout, and with the missile flying at small angles-of-attack, the probe is extended. With the probe extended, as shown in Figure 1-2, the aerodynamic drag is reduced; thus the decay of missile velocity is decreased. The range of possible Mach numbers was considered to be Mach 1.4 to Mach 2.0 at small angles-of-attack.

B. THESIS PURPOSE

The purposes of this thesis are: (1) to evaluate theoretically the static pressure probe general designs developed by Pinckney [1] for use in the Mach 1.4 to Mach 2.0 range; (2) to develop pressure distributions along the probe, and select the probe design best suited to this Mach number range; (3) to evaluate experimentally the probe pressure-sensing performance as an integral part of the missile nose (with probe extended); and (4) to report on experimentation in the Naval Postgraduate School supersonic wind tunnel utilizing the existing Mach 1.4 and Mach 2.0 nozzle blocks.

II. THEORY

A. STATIC PRESSURE PROBE DESIGN

Pinckney [1] discusses the design, for supersonic flow, of a short static pressure probe that is relatively insensitive to angle-of-attack. The general probe design, which is illustrated in Figure 2-1, consists of a conical nose followed by a parabolic tangent ogive fairing the nose into a second, truncated cone. The second cone mates with the cylindrical afterbody of the probe. The parabolic formula used for the tangent ogive section was of the form:

$$\frac{Y}{R_n} = \pm \left[A\left(\frac{X}{R_n}\right)^2 + B\left(\frac{X}{R_n}\right) + C\right]^{\frac{1}{2}} \qquad (2\text{-}1)$$

The value of Y/R_n at the junction between the tangent ogive and the second truncated cone was specified. The conical nose half-angle (β) and the second truncated cone half-angle (ω) were also specified. Based on this information, the constants A, B, and C were calculated. The probe nose half-angle is dependent on the free-stream Mach number, M_∞; the cone angle must be small enough so that shock detachment does not occur. Static pressure holes are located at points where static pressure equals free-stream static pressure. These points of pressure equality vary with the length and angle of the conical nose. Pinckney [1] calculated the theoretical pressure distribution for this general design utilizing a blunt-body program coupled with a method of characteristics program. He made calculations for $\beta = 10$ degrees with ω varying between 2 and 4 degrees

for M_∞ = 2.5 and 4.0 and zero angle-of-attack. Wind tunnel tests were conducted utilizing four different probe types. The first two probe types had β = 10 degrees and ω = 2 or 3 degrees, and were tested at M_∞ = 2.5 and 4. The second two probe types, which had β = 20 degrees and ω = 2.0 or 3.5 degrees, were also tested at M_∞ = 2.5 and 4. Tests were conducted at attack angles ranging from 0 to 12 degrees.

Figure 2-2, which is reproduced from Kuethe and Chow [2], is a graph of shock angle versus Mach number for various cone angles. Since the thrust of this research concerns Mach numbers between 1.4 and 2.0, Figure 2-2 shows that β cannot be greater than approximately 15 degrees, or shock wave detachment will result at M_∞ = 1.4. Therefore, a conical nose half-angle of β = 10 degrees was chosen. Pinckney's theoretical results for β = 10 degrees, which are shown in Figure 2-3, indicate that the pressure distribution which most closely approximates that of the free-stream static pressure will be obtained with ω = 3 degrees at M_∞ = 2.5. Pinckney's experimental results, which are shown in Figure 2-4, indicate close agreement with the theoretical calculations. Figure 2-5 illustrates Pinckney's probe design for β = 10 degrees and ω = 3 degrees. Since Pinckney's theoretical calculations were for much higher Mach numbers, it was considered prudent, for research completeness, to obtain theoretical values for the static pressure distribution at lower Mach numbers. For consistency, attempts were made to obtain the computer program used by Pinckney [1]; however, the program was not immediately available. Therefore, an alternative approach was sought. The coefficients of the parabolic tangent ogive sections for β = 10 degrees and ω = 3 degrees were readily available and were provided by Mr. Pinckney. The values of the coefficients are as follows: A = -0.009267312, B = 8.3676155,

and C = -402.88107. The coefficients were verified, and Eq. 2-1 provides the ogive section body shape used in the theoretical work described in the next section.

B. STATIC PRESSURE DISTRIBUTION

Gawain and Schonberger [3] discuss small perturbation supersonic flow theory applied to a body of revolution. The theory presented in Ref. 3 is essentially that of classical slender-body small-perturbation theory, with corrected boundary conditions in the sense that the boundary conditions are applied at the body surface. In more elementary theory, the boundary conditions are applied along the axis of the body. The use of the exact boundary conditions yields more accurate solutions than those obtained from more elementary theory. The theory of Ref. 3 was considered adequate for the purposes of this thesis, as only small angles-of-attack were considered. A BASIC language computer program, suitable for use on a microprocessor, was developed based on the theory and calculation procedures in Ref. 3. The program, and a sample data run for $M_\infty = 2.0$ at angle-of-attack $\alpha = 0$ and 10 degrees, are given in Appendix A.

C. RESULTS OF THEORETICAL CALCULATIONS

1. Theoretical Calculations

The pressure distribution was calculated for $M_\infty = 1.4$, 1.6, 1.8, 2.0, and 2.5 at zero angle-of-attack (α). The $M_\infty = 2.5$ calculations served as a comparison between Pinckney's theoretical and experimental results [1] and the theory used in this research. Figure 2-6 is a graph of P/P_∞ versus X/R_n for $M_\infty = 2.5$, $\beta = 10$ degrees, and $\omega = 3$ degrees. Comparing Figures

2-3 and 2-6, it can be seen that the graph shapes are the same; however, the theoretical results depicted in Figure 2-6 are slightly higher than those of Figure 2-3 (approximately 2.7 percent). Yet, in comparing Figure 2-6 with the experimental results of Figure 2-4, only a 1 percent difference exists.

In addition to the calculations above, computations were made for angles-of-attack α = 1, 2, 4, 6, 8, and 10 degrees at M_∞ = 1.4, 1.6, 1.8, and 2.0. The calculation procedure and results will be discussed in Section 4, below.

2. Probe Pressure Hole Location

As was discussed previously, in Part A of this chapter, optimum probe pressure hole location depends on the free-stream Mach number. Due to the range of Mach numbers, a design compromise is made that minimizes the pressure error over the range of M_∞ rather than for one specific M_∞. Figure 2-7 is a graph of P/P_∞ versus X/R_η for M_∞ = 1.4, 1.6, 1.8, and 2.0, at zero angle-of-attack. The graph shows clearly that the minimum difference in P/P_∞ for the range of M_∞ occurs at approximately X/R_η = 260. The difference in P/P_∞ due to variable M_∞ is approximately 4 percent.

3. Error in Altitude Due to Error in Pressure Measurement

Pressure as a function of altitude is given by:

$$P = P_0 e^{-\xi h} \quad , \qquad (2\text{-}2)$$

where $\xi = (7.6\ \text{km})^{-1}$ and P_0 is the pressure at sea level. Eq. 2-2 was obtained by graphing pressure versus altitude using data from the *U. S. Standard Atmosphere, 1976* [4], and fitting a curve to the data. Taking the

natural logarithm of both sides of Eq. 2-2 yields:

$$\ln P = -\xi h + \ln P_0 \quad . \tag{2-3}$$

Since $P_0 = 1$ atmosphere, Eq. 2-3 becomes:

$$\ln P = -\xi h \quad . \tag{2-4}$$

To find the error in altitude due to the difference in pressure, the derivative of Eq. 2-4 is taken, which gives:

$$dP/P = -\xi dh \quad . \tag{2-5}$$

Rearranging Eq. 2-5, the altitude error becomes:

$$dh = -\frac{1}{\xi} \cdot dP/P \quad . \tag{2-6}$$

With $1/\xi = 7.62$ km and $dP/P = 0.04$, the value of dh is 300 meters, or 984 feet. This error is well within the tolerance specified for probe performance, i.e., 25,000 feet ± 2,000 feet.

4. Probe Pressure Readings at Angle-of-Attack

Figure 2-8 shows a cross section of the static pressure probe. The static pressure hole on the windward side is number 1, while the hole on the leeward side is number 3. Using the principle of conservation of mass, the mass flow rate in, $\dot{m}_i$, must equal the mass flow rate out, $\dot{m}_o$; therefore:

$$\rho_1 V_1 A_1 + 2\rho_2 V_2 A_2 + \rho_3 V_3 A_3 = 0 \quad . \tag{2-7}$$

Since $\rho_1 = \rho_2 = \rho_3$ and $A_1 = A_2 = A_3$, Eq. 2-7 reduces to:

$$V_1 + 2V_2 + V_3 = 0 \quad . \tag{2-8}$$

Note that Eqs. 2-7 and 2-8 require the velocity to be an algebraic quantity: a flow into the probe is defined as positive. Streeter and Wylie [5] demonstrate that flow through an orifice can be represented by:

$$P_0 - P = \tfrac{1}{2} C \rho V^2 \quad , \tag{2-9}$$

where P_0 is the pressure upstream of the orifice, P is the pressure downstream of the orifice, and C is a constant for incompressible flow. Writing Eq. 2-9 in terms of the parameters of Figure 2-8 yields:

$$|P_1 - P_p| = \tfrac{1}{2}\rho_1 V_1^2 C_1 \tag{2-10}$$

$$|P_2 - P_p| = \tfrac{1}{2}\rho_2 V_2^2 C_2 \tag{2-11}$$

$$|P_3 - P_p| = \tfrac{1}{2}\rho_3 V_3^2 C_3 \quad , \tag{2-12}$$

where P_p is the pressure measured by the probe and C is the flow coefficient for pressure drop across the pressure holes. Solving Eqs. 2-10, 2-11, and 2-12 for V_1, V_2, and V_3, respectively, and substituting into Eq. 2-8, yields:

$$[2|P_1 - P_p|]^{\frac{1}{2}} \pm 2[2|P_2 - P_p|]^{\frac{1}{2}} \pm [2|P_3 - P_p|]^{\frac{1}{2}} = 0 \quad . \tag{2-13}$$

Simplification to this form was made possible because $\rho_1 = \rho_2 = \rho_3$ and $C_1 = C_2 = C_3$. Note that the value of C is not needed, since C cancels in Eq. 2-13.

Eq. 2-13 is nonlinear, and its eight mathematically possible cases are shown in Table 2.1. A plus sign (+) indicates flow into the probe; a minus sign (-) indicates flow out of the probe. Some cases which are mathematically possible but not physically possible can be eliminated.

Case	P_1-P_p	P_2-P_p	P_3-P_p
1	+	+	+
2	-	+	+
3	+	-	+
4	+	+	-
5	+	-	-
6	-	+	-
7	-	-	+
8	-	-	-

Table 2.1 Mathematically Possible Cases for Eq. 2-13

Cases 1 and 8 can be eliminated immediately as not satisfying conservation of mass. In addition, at positive angles-of-attack (i.e., probe tip up), the pressure P_1 will be higher than P_2 or P_3. Therefore, cases 2, 6, and 7 may be ruled out as not possible. An iterative computer program was written to solve Eq. 2-13 for P_p, given that cases 3, 4, and 5 are the only possible cases. A listing of the program and a sample data run can be found in Appendix B.

Figure 2-9, which plots P/P_∞ as a function of α, shows probe theoretical performance for values of α ranging between zero and ten degrees. The data in Figure 2-9 were calculated for $M_\infty = 1.4$ and for $M_\infty = 2.0$.

III. EXPERIMENTAL APPARATUS

A. WIND TUNNEL

1. Mach 2.0 Wind Tunnel Tests

Wind tunnel tests were conducted in the Naval Postgraduate School 4 x 4 inch supersonic wind tunnel using the existing Mach 2.0 nozzle blocks. (The Mach number of 2 is nominal; the actual Mach number is 1.92). Figures 3-1 and 3-2 are two photographs of the general experimental apparatus. They present two views of the supersonic wind tunnel and its associated instrumentation. Utilizing a one-fifth scale model, and regulating wind tunnel stagnation pressure, an actual Reynolds number of $Re = 1.3 \times 10^5$ was attainable, which compares favorably with the Reynolds number for the full-scale probe at 25,000 feet (viz., $Re = 4.3 \times 10^5$). The reference length for the calculation of the Reynolds number is 0.020 meters. Twenty-three wind tunnel tests were conducted at $M_\infty = 1.92$ with $\alpha = 0, 1, 2, 4, 6, 8,$ and 10 degrees.

Prior to any testing, the fine-mesh wire screen in the wind tunnel plenum was discovered to be torn, and hanging loose in the plenum chamber. The screen serves to insure a flat velocity profile (flat stagnation pressure profile) and to generate small-scale turbulence which dissipates prior to arrival at the test section. The plenum chamber exterior can be seen in Figure 3-1. Sufficient manpower to replace the plenum chamber screen was not available. Therefore, the screen was removed. To verify that the flow in the wind tunnel test section was uniform, an additional pressure tap was installed opposite one of the existing pressure taps.

Testing showed no significant pressure difference (approximately 0.5 percent) between the two pressure taps. Therefore, the pressure measurements suggest that the test section velocity profile was reasonably uniform at Mach 2.0.

2. Mach 1.4 Wind Tunnel Tests

Tests were attempted utilizing the existing Mach 1.4 nozzle blocks. Supersonic flow could not be established in the test section. Appendix C provides a sequential listing of testing attempts and corrective measures taken between tests, and discusses the three most probable reasons for testing failure.

3. Mach 1.51 Wind Tunnel Tests

Since experimental data at a lower Mach number were still desired, various alternatives were explored. The four alternatives investigated were: (1) to replace the plenum chamber screen; (2) to design and manufacture Mach 1.5 nozzle blocks; (3) to enlarge the existing Mach 1.4 nozzle block second throat by machining; or (4) to attempts tests using a combination of Mach 1.4 and Mach 2.0 nozzle blocks. Alternatives 1 through 3 were ruled out due to inadequate manpower, funding, and/or research time. Alternative 4 was attempted. Testing in this unorthodox manner was attempted in order to verify that the missile nose shock did not detach at a lower Mach number. Two shock waves occur at the nose of the missile with the probe extended. A nearly conical shock is attached to the probe. A curved shock wave originates due to the missile ogive; this curved shock wave is termed the missile nose shock. The probe conical shock and missile nose shock merge to form the bow shock wave. The probe conical shock, missile nose shock, and resulting bow shock wave can be seen in Figure 3-3, which is a photograph of

the model mounted in the wind tunnel. The probe is oriented at zero angle-of-attack, and the flow is at $M_\infty = 1.92$. Both the probe conical shock wave and the missile nose shock wave are attached. If the missile nose shock moves upstream of the probe pressure ports, erroneous pressure readings are obtained.

The Mach number gradient in the wind tunnel test section resulting from the combination of nozzle blocks was calculated using the method of characteristics found in Liepmann and Roshko [6]. Figure 3-4 shows the Mach number gradient in the test section and the shock waves that result using the combination of nozzle blocks. Figure 3-5 is a photograph of the Mach 2.0 and Mach 1.4 nozzle blocks installed in the wind tunnel. The theoretical Mach number obtained using this combination of nozzle blocks was $M_\infty = 1.51$ at the probe nose, $M_\infty = 1.538$ at the top, and $M_\infty = 1.16$ at the bottom of the wind tunnel test section. Experimental results, which are discussed in Chapter IV, were used to verify theory.

B. MODEL DESIGN

A one-fifth scale model of the static pressure probe and missile nose was used. Since a complete model could not be mounted in the tunnel, the missile nose was truncated at 40 percent of the nose length. Maximum model size was dictated by maximum allowed wind tunnel blockage (approximately 6.4 percent) at Mach 1.4. The allowed wind tunnel blockage limited the combined frontal area of the model and mounting system. Pinckney [1] supplied the drawings for the static pressure probe. The Naval Weapons Center, China Lake, California, provided the formula and coefficients for the Von Karmen ogive missile nose. The Von Karmen ogive is given by:

$$Y = \frac{R}{\sqrt{\pi}} \cdot \left[\cos^{-1}\left(1 - \frac{2X}{L}\right) - \tfrac{1}{2}\sin\left(2\cos^{-1}\left(1 - \frac{2X}{L}\right)\right)\right]^{\frac{1}{2}} \qquad (3\text{-}1)$$

for the full-scale missile, where R = 2.5 inches and L = 10 inches. Figure 3-6 is a front view of the model and double-wedge airfoil used to mount the model in the wind tunnel. Design compromises between the maximum missile nose diameter and maximum wedge thickness were required to remain within wind tunnel blockage limits. The maximum diameter of the model nose used is 0.792 inches, and the maximum wedge thickness is 0.165 inches. The mounting wedge length is 3.900 inches, and a wedge half-angle of 9 degrees was utilized to prevent oblique shock detachment at Mach 1.4. The frontal area of the model plus mounting system was 1.005 square inches, which is within the allowed wind tunnel blockage. Figure 3-7 is a photograph of the model ogive nose and the extended static pressure probe. The ogive is 1.200 inches in length. The pressure probe extends 0.680 inches from the missile nose. Figure 3-8 is a photograph of the static pressure probe mated to the missile nose. The four probe pressure holes are 90 degrees apart and 0.0135 inches in diameter, and are located 0.1325 inches from the probe conical nose tip. The parabolic tangent ogive and second truncated cone start at 0.0525 inch and 0.1225 inch, respectively, from the probe nose tip, and are made of 0.060-inch outside diameter, 0.040-inch inside diameter stainless steel tubing. The probe nose cone through the second truncated cone is made of 0.0625-inch diameter hole on centerline. After machining, the drill rod is mated to the stainless steel tubing with silver solder. Figure 3-9 is a photograph of the top view of the model and mounting wedge. Figure 3-10 is a photograph of the model mounted in the wind tunnel, and Figure 3-11 is a close-up of the model mounted in the wind tunnel test section.

C. INSTRUMENTATION

Pressure taps in the wind tunnel wall and on the model surface were connected to a Giannini 12-position scanivalve with Tygon tubing. The scanivalve has a range from absolute zero to 100 PSIA. The scanivalve was connected to a Gould Statham absolute pressure transducer, Model PA732TC-100-350. The transducer was powered by a five-volt excitation; it has a pressure range from absolute zero to 100 PSIA, with a maximum frequency response of 8,700 Hz. A variable-gain differential amplifier conditioned the transducer output to an Analog Devices 4½-digit voltmeter. The voltage displayed is directly proportional to the pressure. Transducer calibration was accomplished utilizing a 60-inch mercury column and vacuum pump. For higher pressure, a Wallace and Tiernan bourdon tube absolute pressure gauge was used (range absolute zero to 100 PSIA). Schlieren photographs of the flow, including shock waves, were taken. A 1,000-watt mercury vapor light source and a reflex-type camera converted to accept Polaroid Type 152 film were used.

IV. EXPERIMENTAL RESULTS

A. MACH 2.0 EXPERIMENTAL RESULTS

1. Data Reduction Technique

Twenty-three wind tunnel tests were conducted at Mach 2.0 with angles-of-attack varying from - 2 to + 10 degrees. Tables 4.1 and 4.2 depict sample wind tunnel test data for α = 0 and 2 degrees, respectively.

Run: 4 P = 29.85 in Hg Date: 24 September 1980
$M_\infty = 1.92$ $\alpha = 0°$ T = 16.2°C Time: 0902

Reading	*Model (PSIG)*	*Port #1 (PSIG)*	*Plenum (PSIG)*
1	-9.37	-9.25	+23.12
2	-9.37	-9.30	+22.82
3	-9.63	-9.49	+22.14
4	-9.77	-9.77	+19.92
5	-9.86	-9.82	+19.27

Table 4.1 Sample Wind Tunnel Data for α *= 0 Degrees and* $M_\infty = 1.92$

Run: 6 P = 29.88 in Hg Date: 24 September 1980
$M_\infty = 1.92$ $\alpha = 2°$ T = 20.5°C Time: 1027

Reading	*Model (PSIG)*	*Port #1 (PSIG)*	*Plenum (PSIG)*
1	-9.12	-9.02	+24.75
2	-9.16	-9.06	+24.58
3	-9.18	-9.10	+24.37
4	-9.21	-9.18	+24.14
5	-9.35	-9.28	+23.90

Table 4.2 Sample Wind Tunnel Data for α *= 2 Degrees and* $M_\infty = 1.92$

The ratio of measured static probe pressure to wind tunnel wall pressure, P/P_∞, was calculated for each set of data points. The arithmetic mean, variance (N weighting), and standard deviation (N weighting) were calculated using the calculation procedure found in Haber and Runyon [7]. Table 4.3 gives these values for various angles-of-attack, α.

Angle-of-Attack	*Theoretical* P/P_∞	*Experimental* P/P_∞	*Experimental Standard Deviation*
0°	1.003	0.987	±0.00861
1°	1.0015	0.984	±0.0102
2°	0.996	0.987	±0.0097
4°	0.976	0.978	±0.0122
6°	0.952	0.974	±0.008
8°	0.938	0.932	±0.013
10°	0.918	0.927	±0.016

Table 4.3 Angles-of-Attack Versus Theoretical and Experimental P/P_∞ *for* $M_\infty = 2.0$

2. Static Pressure Probe Performance

Figure 4-1 is a plot of the data listed in Table 4.3. Calculated points are indicated by the letter X, while experimental mean values are denoted by an asterisk (*) and standard deviations are denoted by the character "#". The scale of the ordinate emphasizes greatly any deviation from $P/P_\infty = 1$. Note that an experimental error bar is not shown for angle-of-attack; such an error bar would be horizontal. Pressure measurements for angles-of-attack of - 1 and - 2 degrees are included in the measurements shown for α = 1 and 2 degrees. A change in α from + 2 to - 2 degrees had little or no effect on pressure measurements. Figure 4-3 shows that

probe performance is reasonably constant in the range $\alpha = 0$ to 6 degrees; the corresponding values of mean P/P_∞ are 0.987 and 0.974. For angles-of-attack greater than 6 degrees, the measured pressure ratio is 1.6 percent less than that predicted by the theory. The mean value of the measured pressure ratio is almost exactly that of the theory at $\alpha = 4$ degrees; at $\alpha = 6$ degrees, the measured P/P_∞ is 2.6 percent greater than theoretical predictions.

Using Eq. 2-6 with dh = 2,000 feet (609.6 meters) and $1/\xi = 7.62$ kilometers, the fractional change in pressure is 0.08. Therefore, taking experimental uncertainty into consideration, the probe will perform within altitude specifications for angles-of-attack less than or equal to 8 degrees at Mach 2. As stated in Chapter III, Figure 3-3 is a photograph of the model mounted in the wind tunnel. The probe is oriented at zero angle-of-attack, and the flow is at $M_\infty = 1.92$. Both the probe conical shock wave and the missile shock wave are visible and attached. The horizontal lines just above the model are due to condensation within the boundary layer on the inside of the test section window. The dark vertical line aft of and below the model is the shadow of the Tygon tubing used to measure probe pressure. Figure 4-2 is a photograph of the model oriented at $\alpha = +1$ degree within the wind tunnel operating at $M_\infty = 1.92$.

B. MACH 1.51 EXPERIMENTAL RESULTS

Seven wind tunnel tests were conducted using the combination of Mach 1.4 and Mach 2.0 nozzle blocks. The model and plenum pressures, as well as pressures at five static pressure ports located along the wind tunnel wall, were recorded for each wind tunnel test. The static pressure ports extended

from just aft of the nozzle throat to the test section. The position of the static pressure ports relative to the wind tunnel test section is shown in Figure 3-1. The static pressure measurements were used to verify the calculations based on the method of characteristics referred to in Chapter III. The measured static pressure for the seven wind tunnel tests was recorded, grouped by test point, and the arithmetic mean and standard deviation were calculated for each point. Theoretical values and actual experimental values were compared, and are shown in Table 4.4.

Test Point	*Theoretical Pressure (PSIA)*	*Observed Mean Pressure (PSIA)*	*Theoretical Mach Number*	*Percent Pressure Difference*
P_1	5.97	5.60	1.57	5.9
P_2	6.05	6.35	1.56	4.7
P_3	7.41	7.92	1.42	6.5
P_4	8.87	9.12	1.29	2.7
P_5	10.00	10.89	1.20	8.1

Table 4.4 Theoretical and Observed Pressure for a Combination of Mach 1.4 and Mach 2.0 Nozzle Blocks

At Mach 1.5, a pressure difference of approximately 7 percent results in a Mach number change of only 0.05. Therefore, the calculated Mach numbers are accurate within ± 0.05, and a predicted Mach number of $M_\infty = 1.50 \pm 0.05$ at the probe tip appears reasonable. Further evidence supporting a value of $M_\infty = 1.5$ can be seen in Figure 4-3, which is a Schlieren photograph of the model in the wind tunnel test section during one of the test runs. The Mach waves emanating from the top and bottom of the test section are oriented at 38 and 46 degrees, respectively. At Mach angle $\mu = 46$

degrees, the value of M_∞ is 1.38. The probe conical nose shock angles are $\phi_1 = 38$ (top) and $\phi_2 = 46$ (bottom), indicating that the probe is at angle-of-attack. A rough estimate of the angle-of-attack is given by:

$$\alpha = \frac{\phi_2 - \phi_1}{2} \quad . \tag{4-1}$$

With $\phi_1 = 38$ and $\phi_2 = 46$, the value of α is 4 degrees. An accurate value for α would require further study. An angle-of-attack between 4 and 6 degrees was predicted theoretically. Since all shocks in the test section are curved due to Mach gradient, all Mach/shock wave angles were measured locally, i.e., in close proximity to the physical object generating them. In addition, Figure 4-3 shows a shock wave just forward of the probe tip; this shock wave was predicted theoretically, and is shown in Figure 3-4.

Due to the Mach number gradient and confused flow in the test section, the pressure measured by the probe is not accurate, and hence is not relevant. Table 4.5, which presents sample wind tunnel test data with the asymmetric nozzle blocks, is included for completeness only. The unorthodox wind tunnel tests did prove, however, that the missile nose shock will not detach at Mach numbers above 1.5.

Figure 4-4 is a graph of distance versus theoretical Mach number and pressure (PSIA) in the wind tunnel test section. The theoretical pressure is indicated by the character "0". Pressures measured by the probe, and the Mach numbers calculated from the Mach waves emanating from the wind tunnel walls, are also indicated. Moreover, Mach waves at several points in the plane of the probe nose were measured and recorded on the graph.

Run: 4 $\alpha = 4°$ $M_\infty = 1.51$ P = 29.98 in Hg   T = 20.5°C   Date: 14 October 1980   Time: 1615

Reading	*Model*	*Port #1 (PSIG)*	*Port #2 (PSIG)*	*Port #3 (PSIG)*	*Port #4 (PSIG)*	*Port #5 (PSIG)*	*Plenum (PSIG)*
1	-9.27	-8.70	-7.86	-6.18	-4.87	-2.92	+11.53
2	-9.25	-8.64	-7.84	-6.21	-4.94	-3.05	+11.38
3	-9.31	-8.74	-7.95	-6.26	-5.09	-3.30	+11.09
4	-9.42	-8.96	-8.22	-6.56	-5.37	-3.57	+10.19
Mean PSIG	-9.31	-8.76	-7.97	-6.30	-5.07	-3.21	+11.04
PSIA	5.41	5.94	6.73	8.40	9.63	11.51	+25.75
Theoretical PSIA	7.01	6.33	6.43	7.87	9.42	10.62	--
Percent Difference	23	6.2	4.5	6.4	2.2	7.7	--

Table 4.5 Sample Wind Tunnel Test Data for $\alpha = 4$ Degrees and $M_\infty = 1.51$

V. CONCLUSIONS AND RECOMMENDATIONS

A. CONCLUSIONS

The following conclusions result from the static pressure probe study:

1. The static pressure probe of Ref. 1, with $\beta = 10$ degrees and $\omega = 3$ degrees, will, as an integral part of the missile nose, perform within altitude specifications of 25,000 feet ± 2,000 feet at Mach 2.0 at angles-of-attack from - 8 to + 8 degrees.
2. At Mach 2.0, within an angle-of-attack range from 0 to 6 degrees, the probe will measure free-stream static pressure within 4 percent. A 4 percent error in measurement is equivalent to an altitude error of 900 feet.
3. The missile nose shock remains downstream of the probe pressure ports for flight Mach numbers above 1.5.
4. Since the theory predicted probe performance within 2.6 percent at Mach 2.0, and since the theory predicted satisfactory performance at Mach 1.4, the static pressure probe should perform within specifications at Mach 1.4.

B. RECOMMENDATIONS

The minimum operating Mach number for the static pressure probe depends on the position of the missile nose shock wave. At some lower Mach number, the missile nose shock wave moves upstream of the pressure ports. M_m is defined as the minimum Mach number for satisfactory probe operation.

The potential use of the static pressure probe as an altitude-measuring device is limited by the minimum Mach number, M_m, and by excursions in the angle-of-attack. Recommended further studies are as follows:

(1) Replace the missing supersonic wind tunnel plenum chamber screen, design and manufacture a set of Mach 1.4 nozzle blocks with a larger second throat, and test the probe. Determine whether $M_m < 1.4$ or $M_m > 1.4$.

(2) Once the actual flight Mach number has been determined, recalculate the theoretical distribution, if required, and reposition the probe pressure ports to remove the error due to Mach number range--an error presently inherent in probe design.

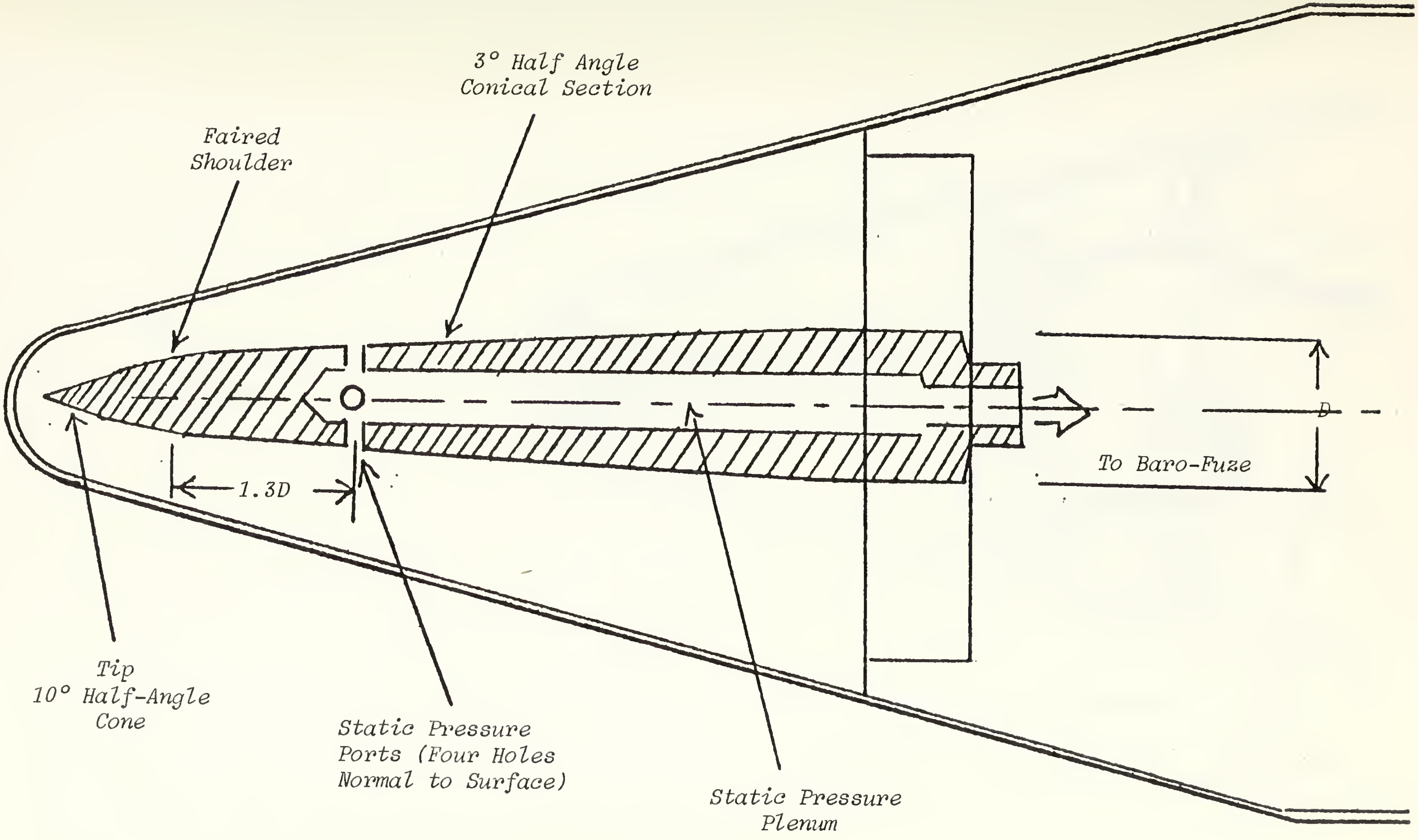
3° Half Angle
Conical Section
Faired
Shoulder
D
To Baro-Fuze
1.3D
Tip
10° Half-Angle
Cone
Static Pressure
Ports (Four Holes
Normal to Surface)
Static Pressure
Plenum

Figure 1-1 Static Pressure Probe Interior to Missile Nose

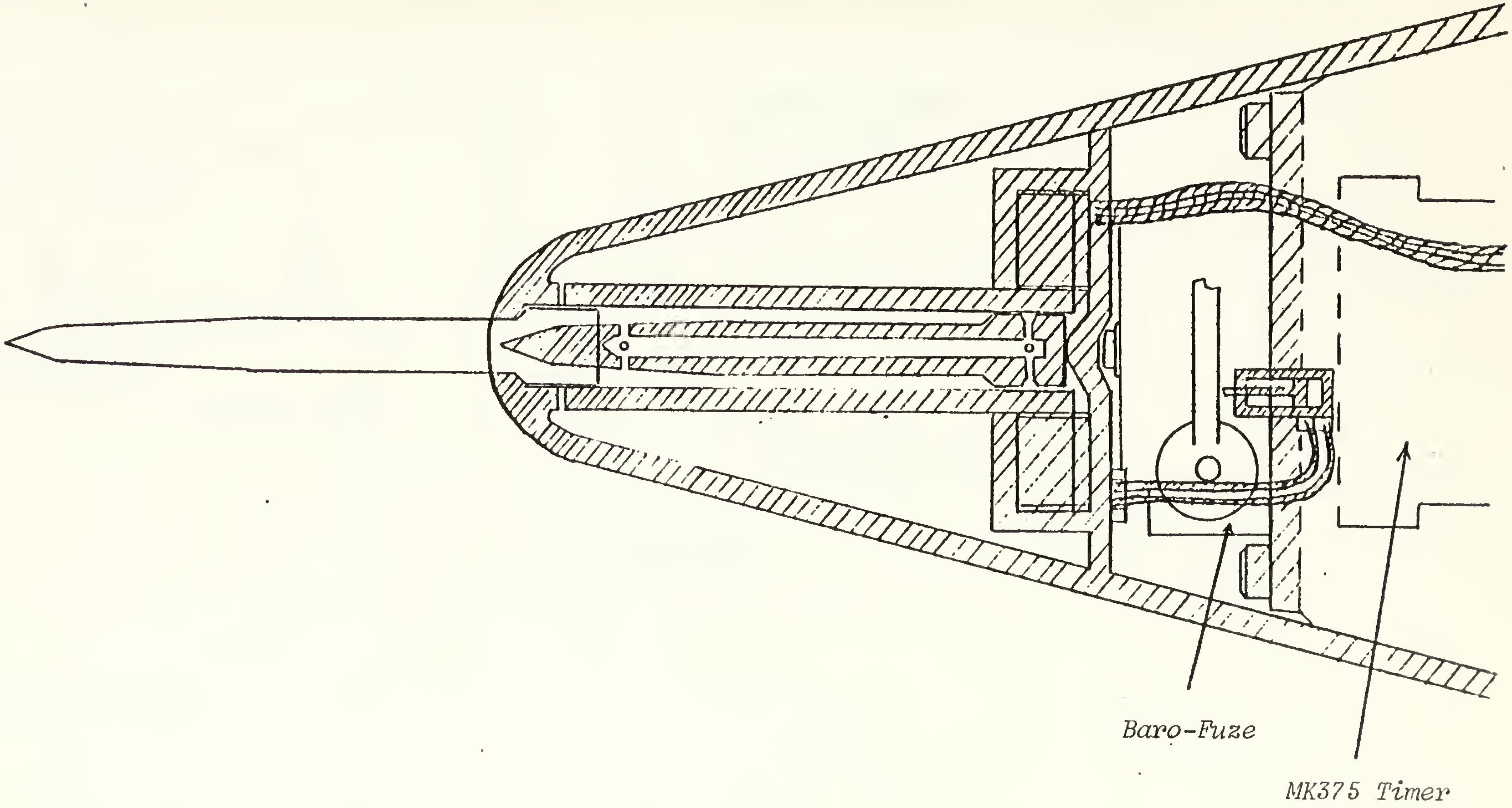
Baro-Fuze
MK375 Timer

Figure 1-2 Static Pressure Probe Both Extended and Interior to the Missile Nose

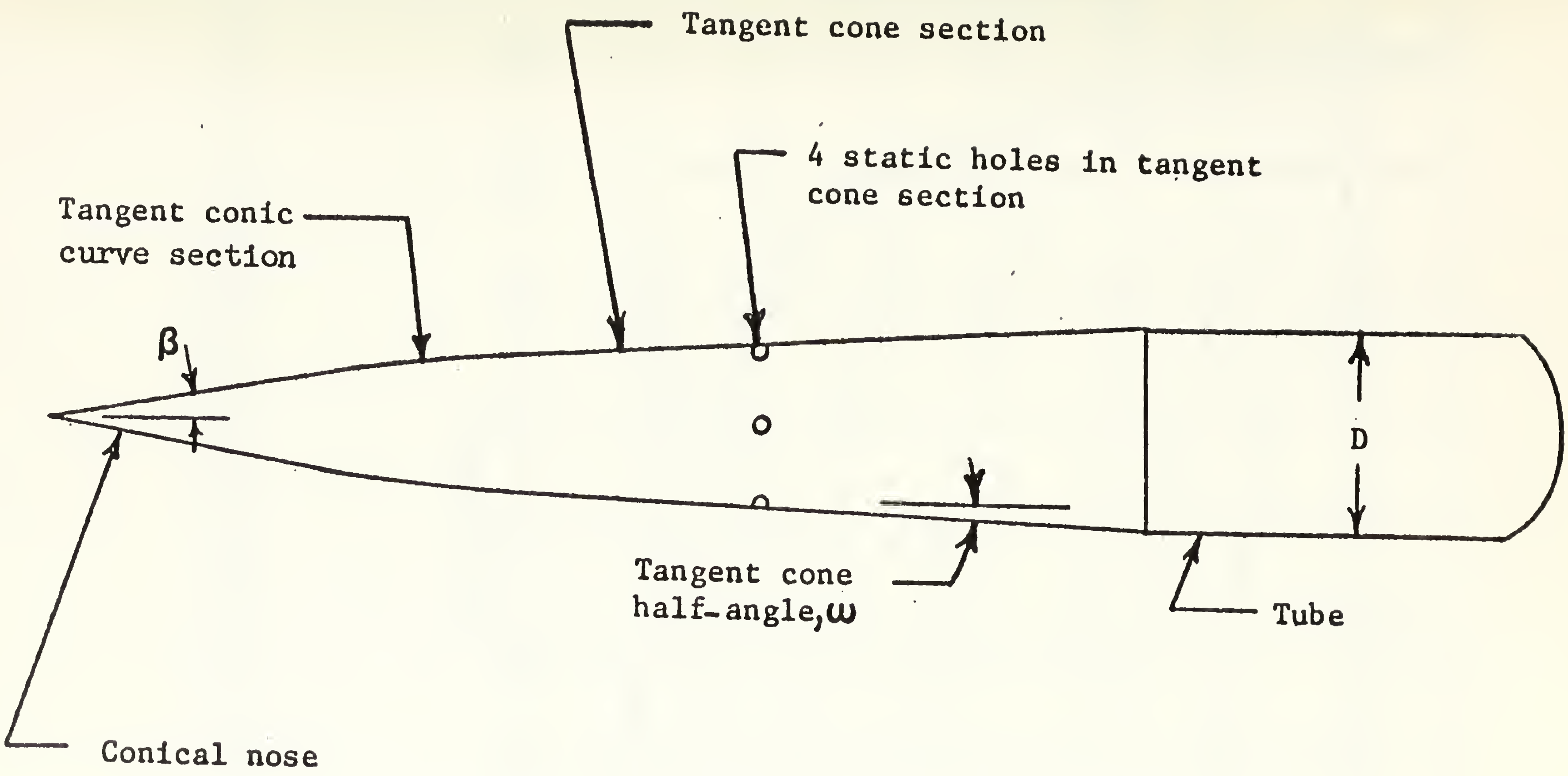
Tangent cone section
4 static holes in tangent cone section
Tangent conic curve section
β
D
Tangent cone half-angle,ω
Tube
Conical nose

Figure 2-1 General Static Pressure Probe Design (Reproduced from Pinckney [1])

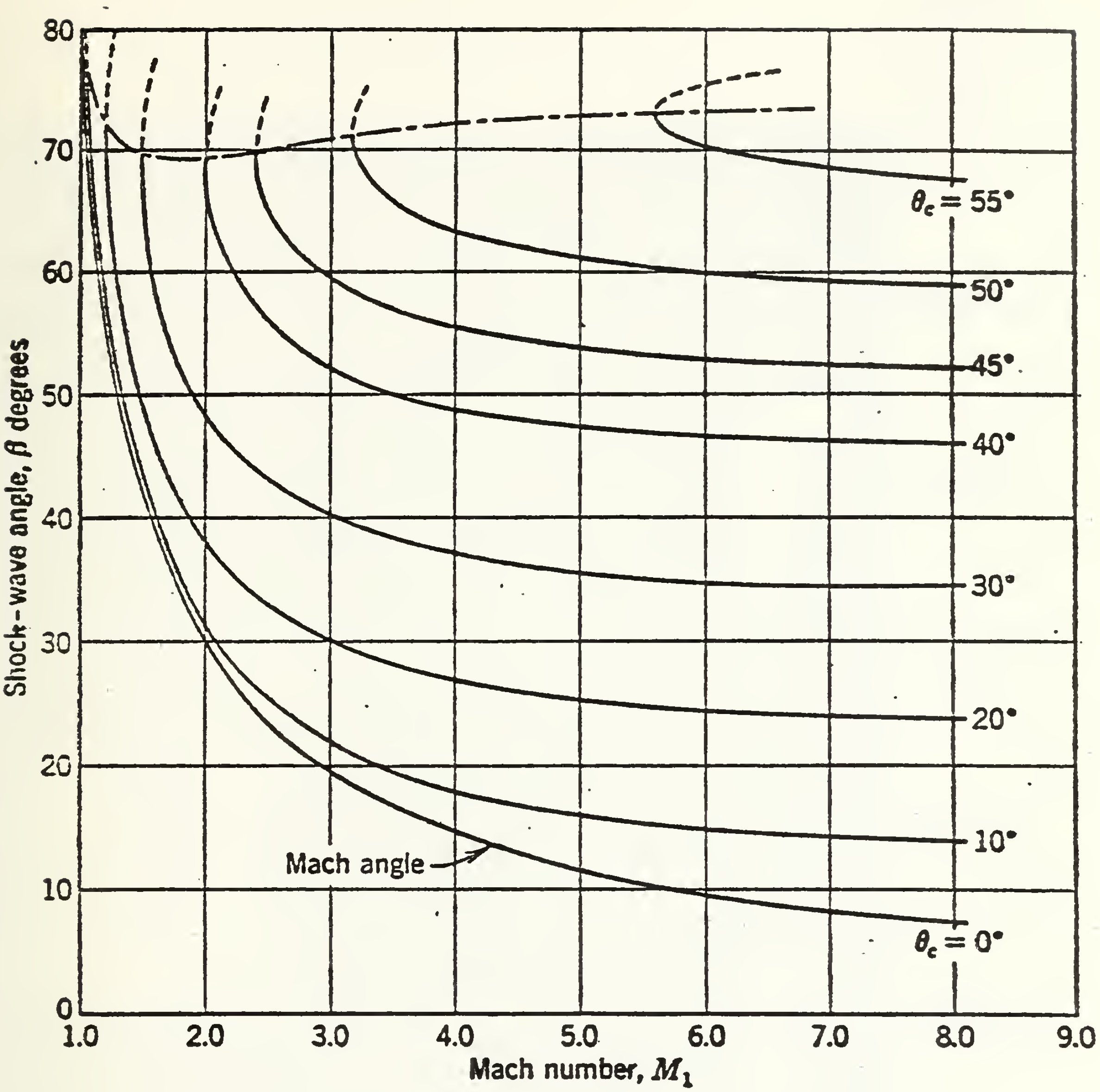

Figure 2-2 Shock Angle Versus Mach Number for Various Cone Angles (Reproduced from Kuethe and Chow [2])

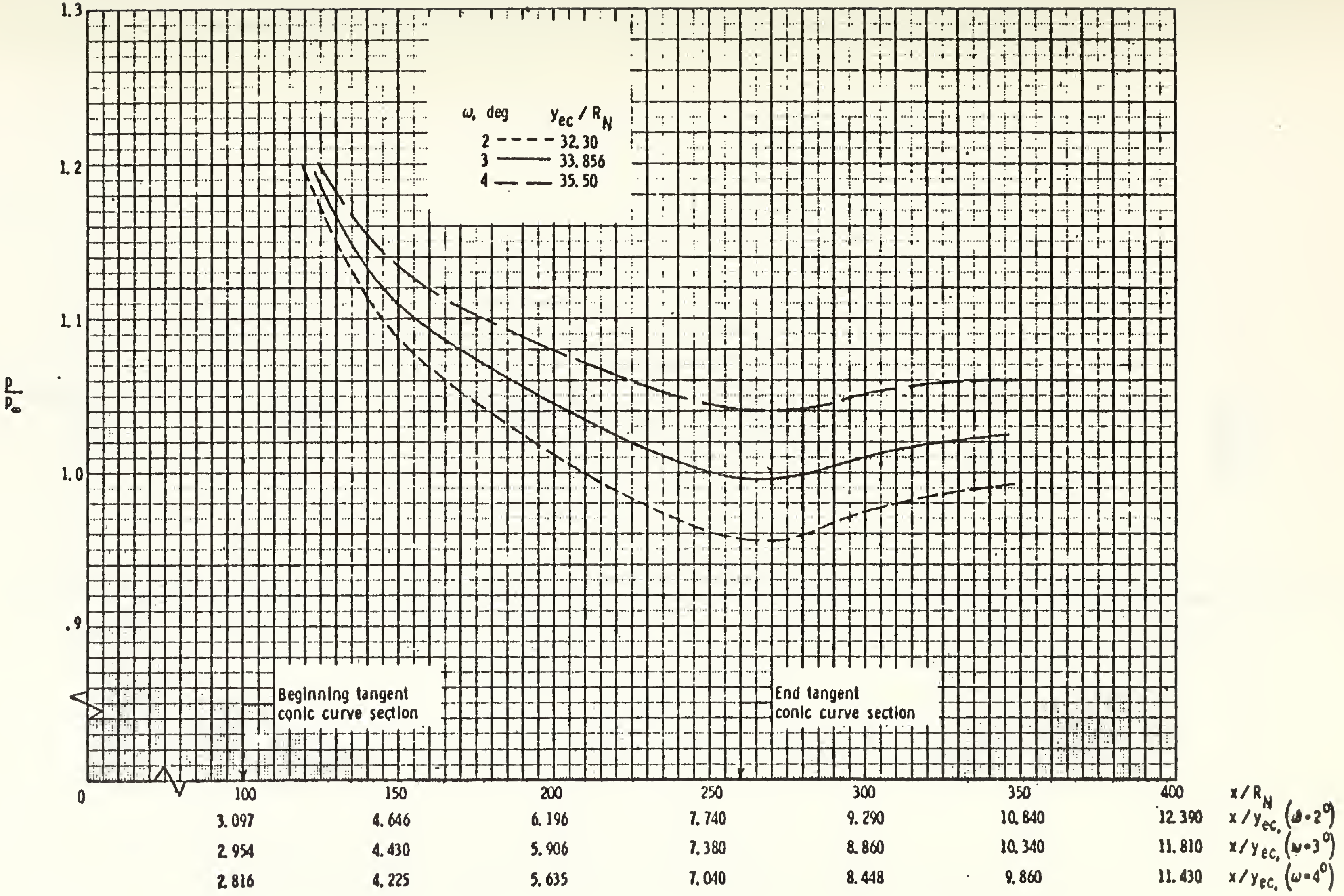

Figure 2-3 Theoretical Static Pressure Distribution as a Function of X/R_n *for* $M_\infty = 2.5$, β *= 10 Degrees, and* ω *= 3 Degrees (Reproduced from Pinckney [1])*

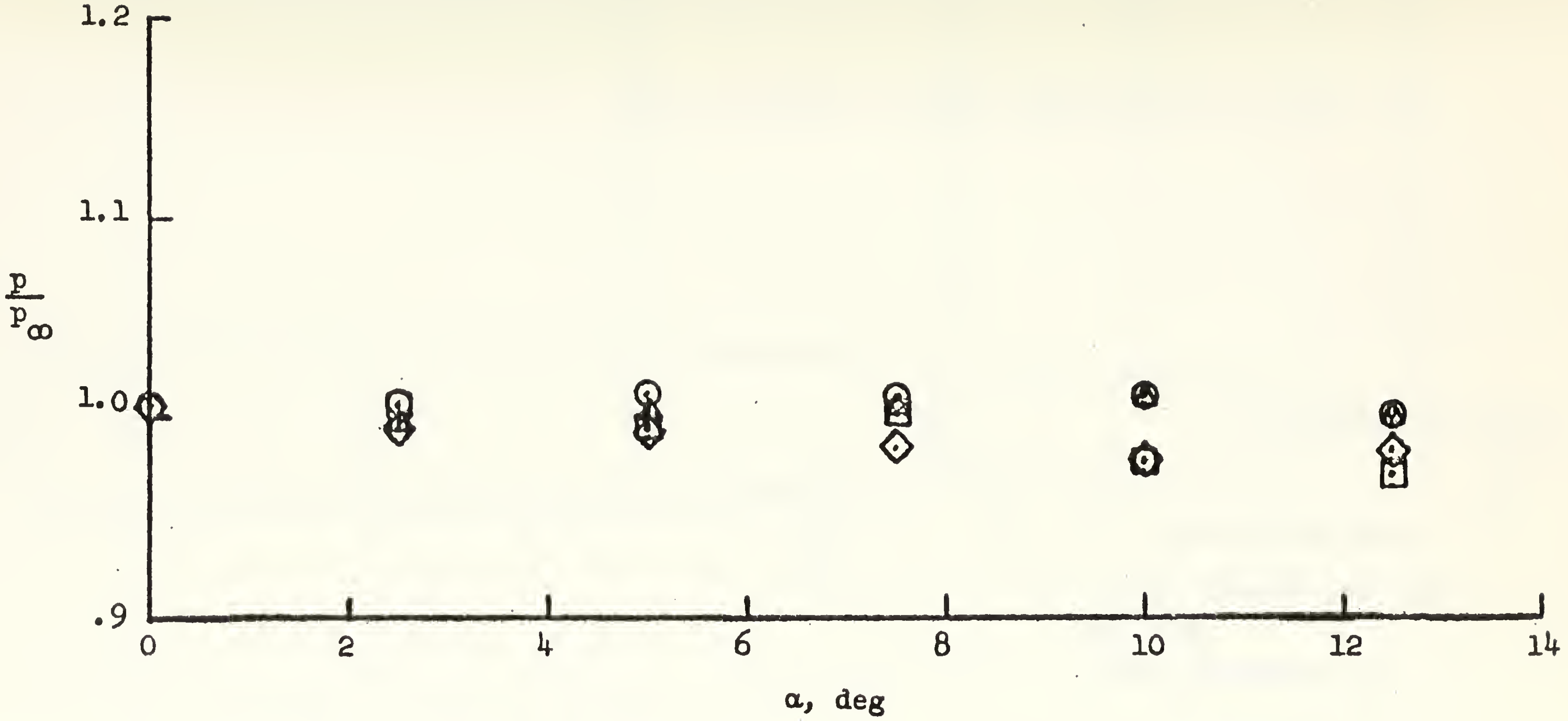

Figure 2-4 Experimental Results of Static Pressure Probe at Angle-of-Attack for $M_\infty = 2.5$, $\beta = 10$ *Degrees, and* $\omega = 3$ *Degrees (Reproduced from Pinckney* [1]*)*

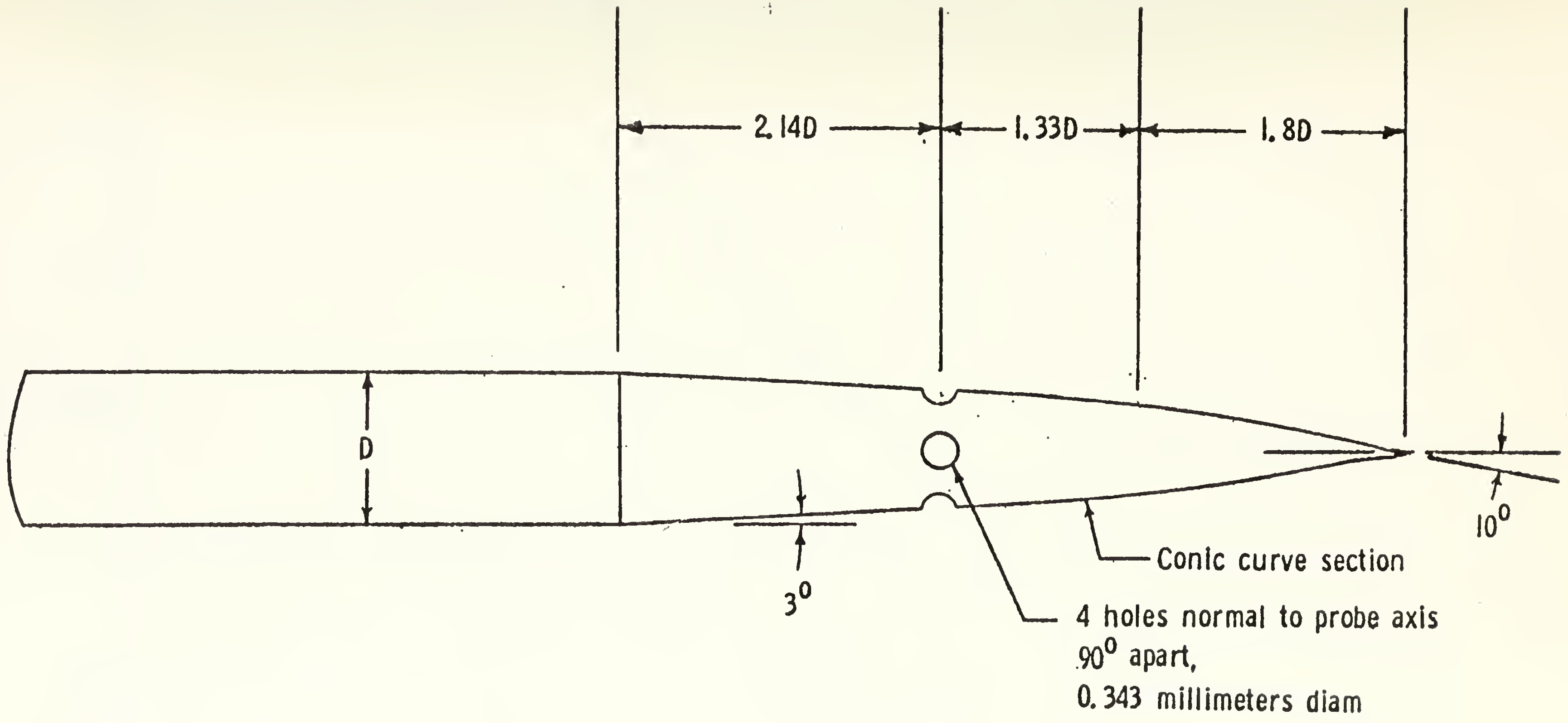
2.14D
1.33D
1.8D
D
3°
10°
Conic curve section
4 holes normal to probe axis
90° apart,
0.343 millimeters diam

Figure 2-5 Static Pressure Probe Design for β = 10 Degrees and ω = 3 Degrees (Reproduced from Pinckney [1])

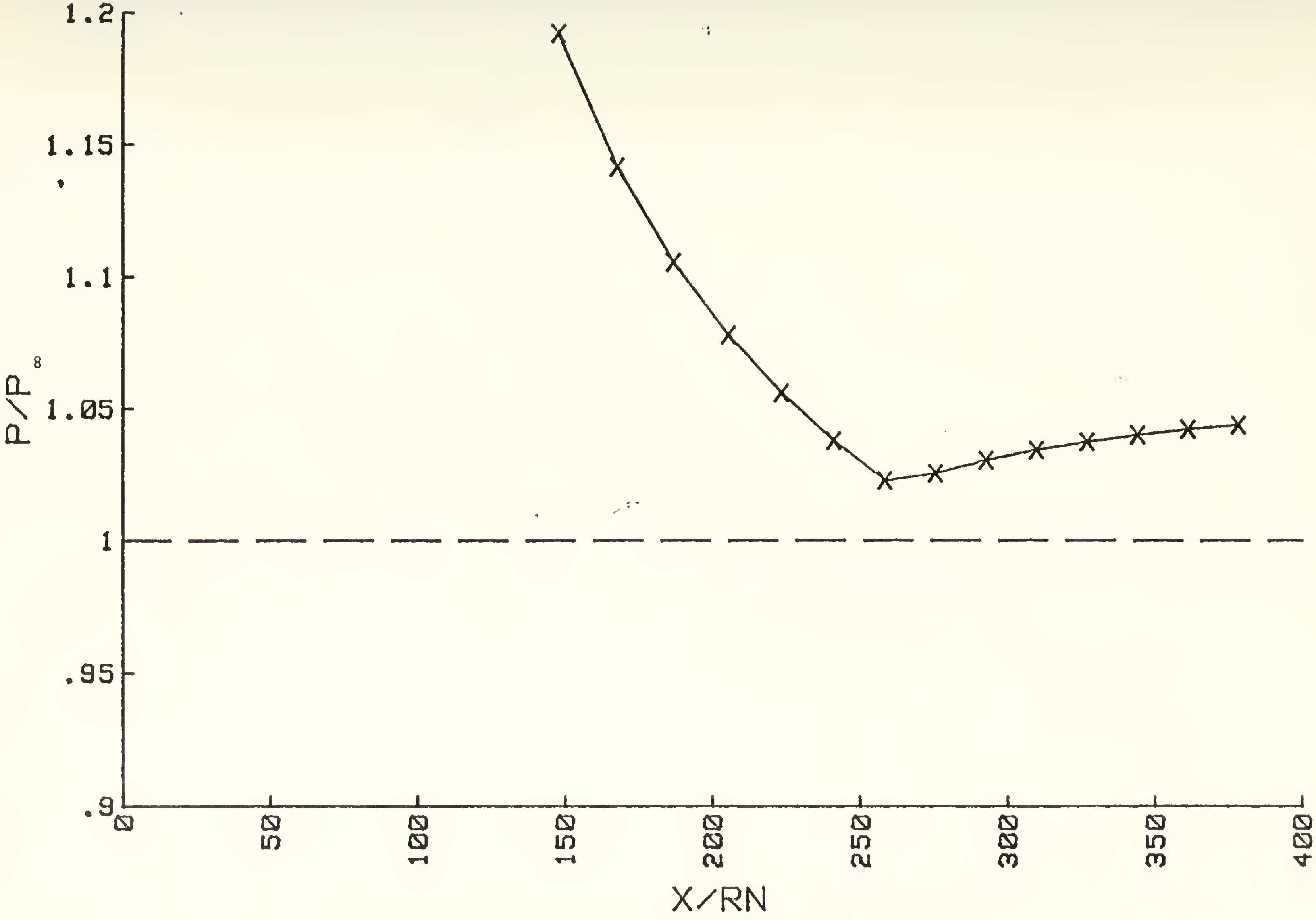

Figure 2-6 *Theoretical Probe Static Pressure Distribution for* M_∞ = *2.5,* β = *10 Degrees, and* ω = *3 Degrees*

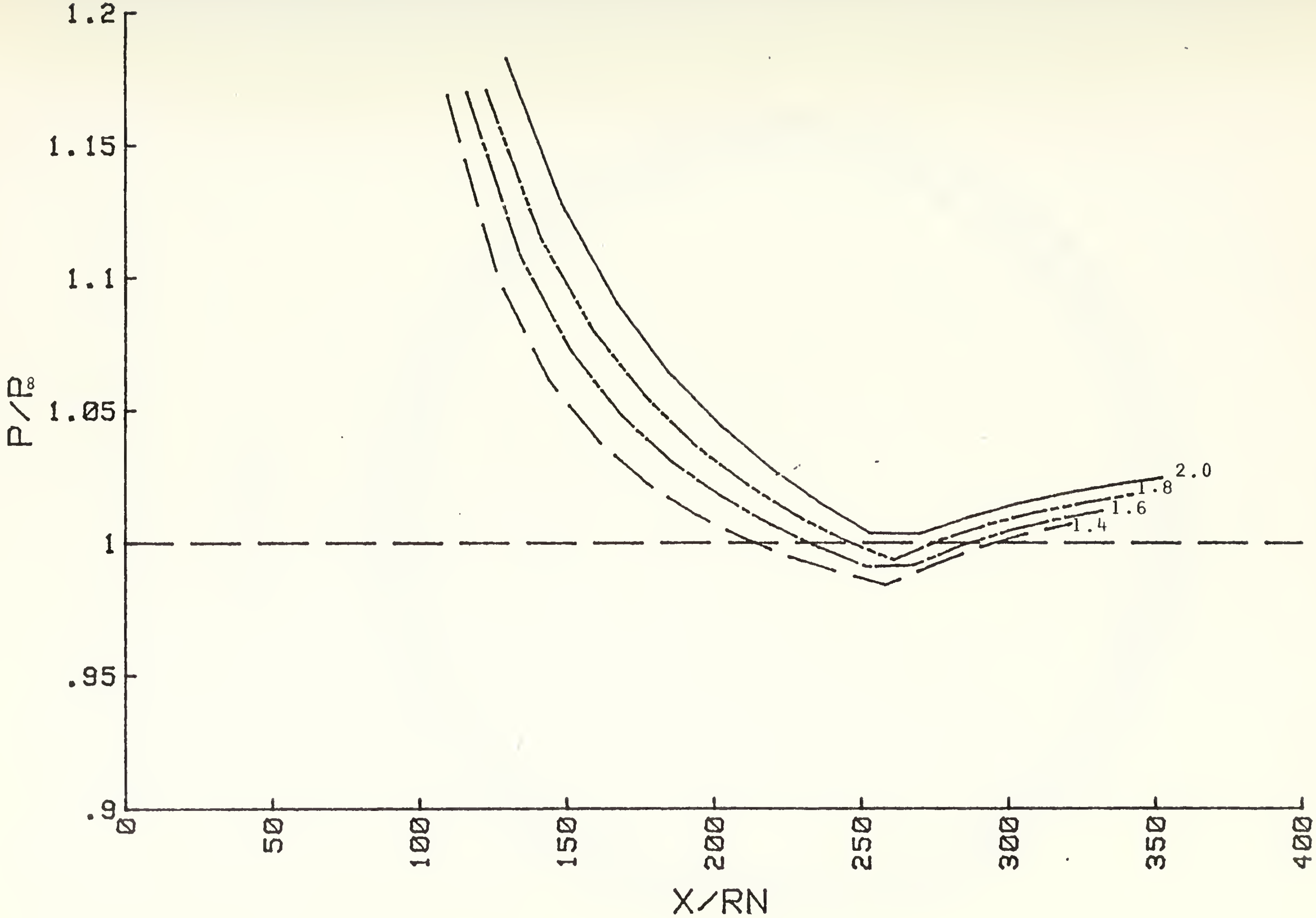

Figure 2-7 Theoretical Probe Static Pressure Distribution for M_∞ *= 1.4, 1.6, 1.8, and 2.0 at Zero Angle-of-Attack*

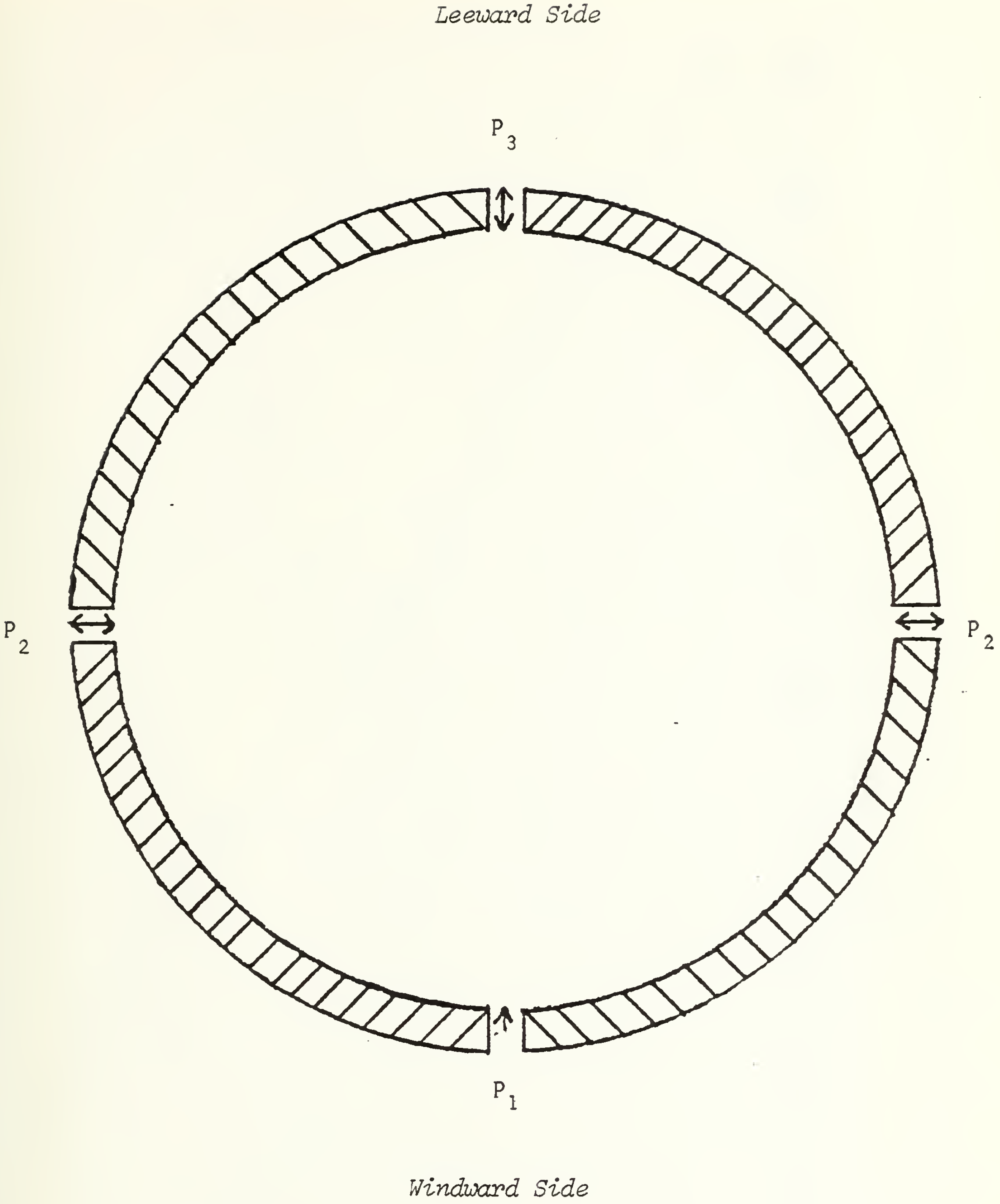
Leeward Side
P_3
P_2
P_2
P_1
Windward Side

Figure 2-8 Static Pressure Probe Cross Section

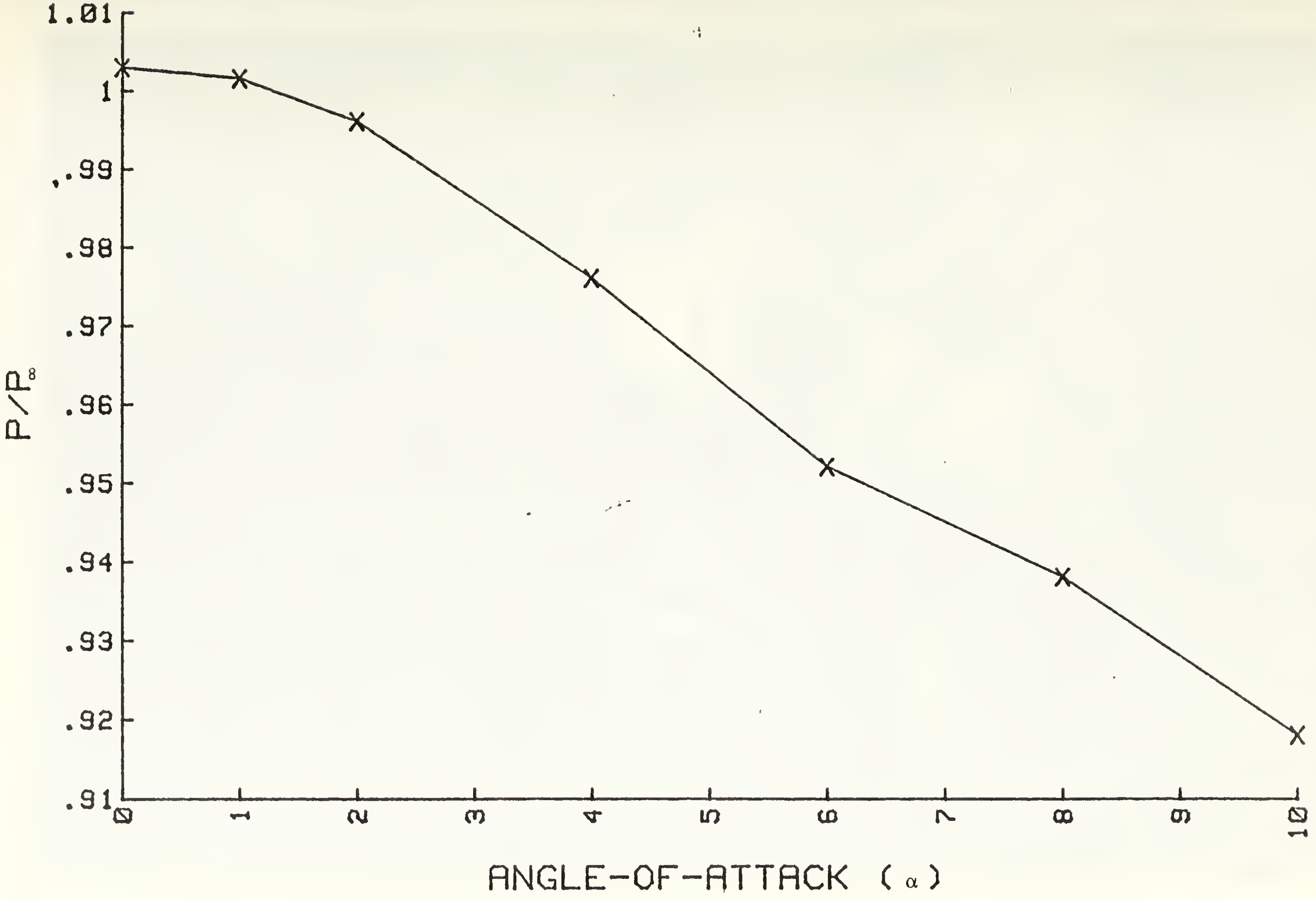

Figure 2-9 Theoretical Probe Static Pressure Distribution as a Function of Angle-of-Attack (α) for $M_\infty = 2.0$

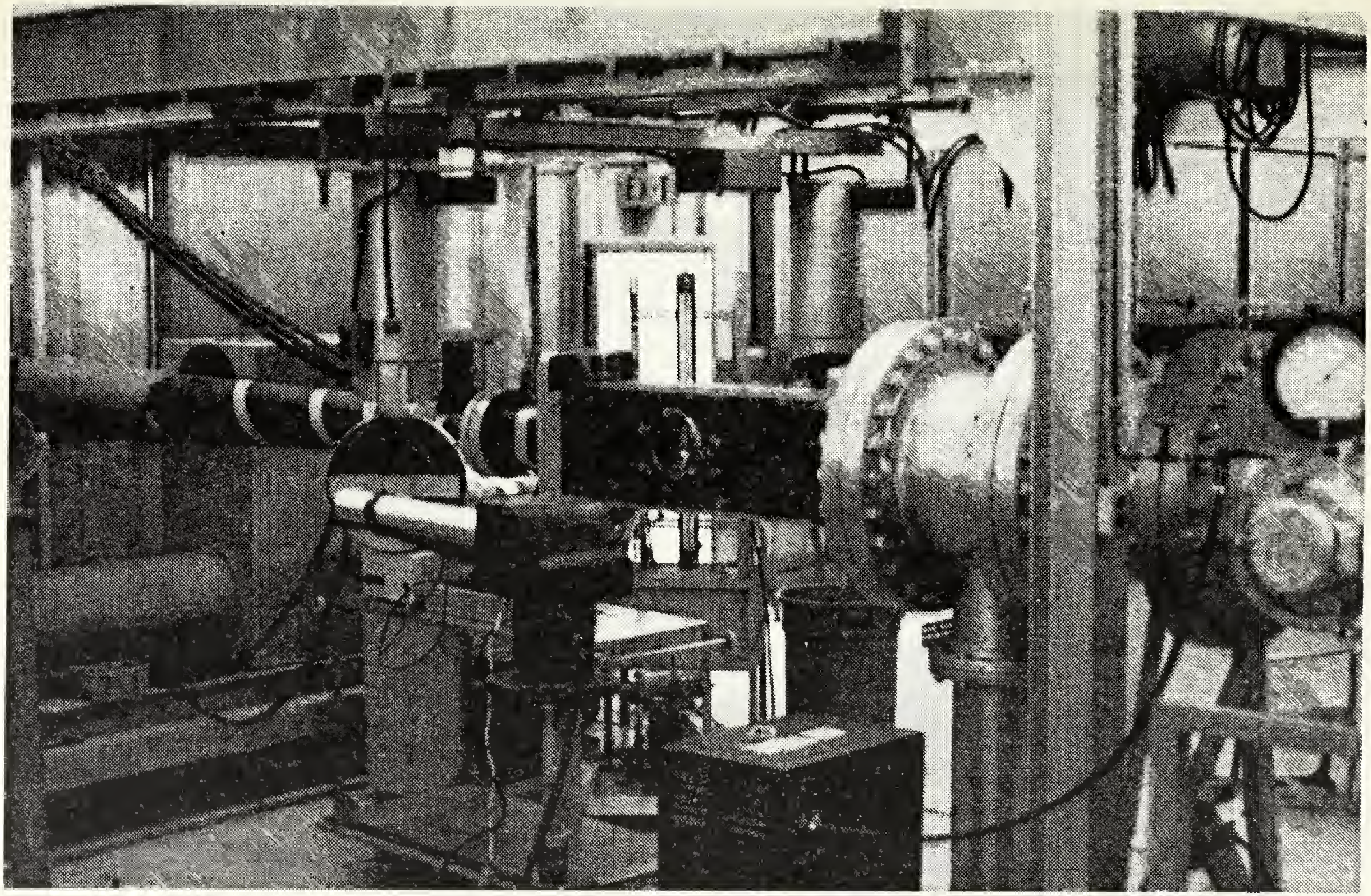

Figure 3-1 Naval Postgraduate School Supersonic Wind Tunnel and Associated Instrumentation (Rear Quarter View)

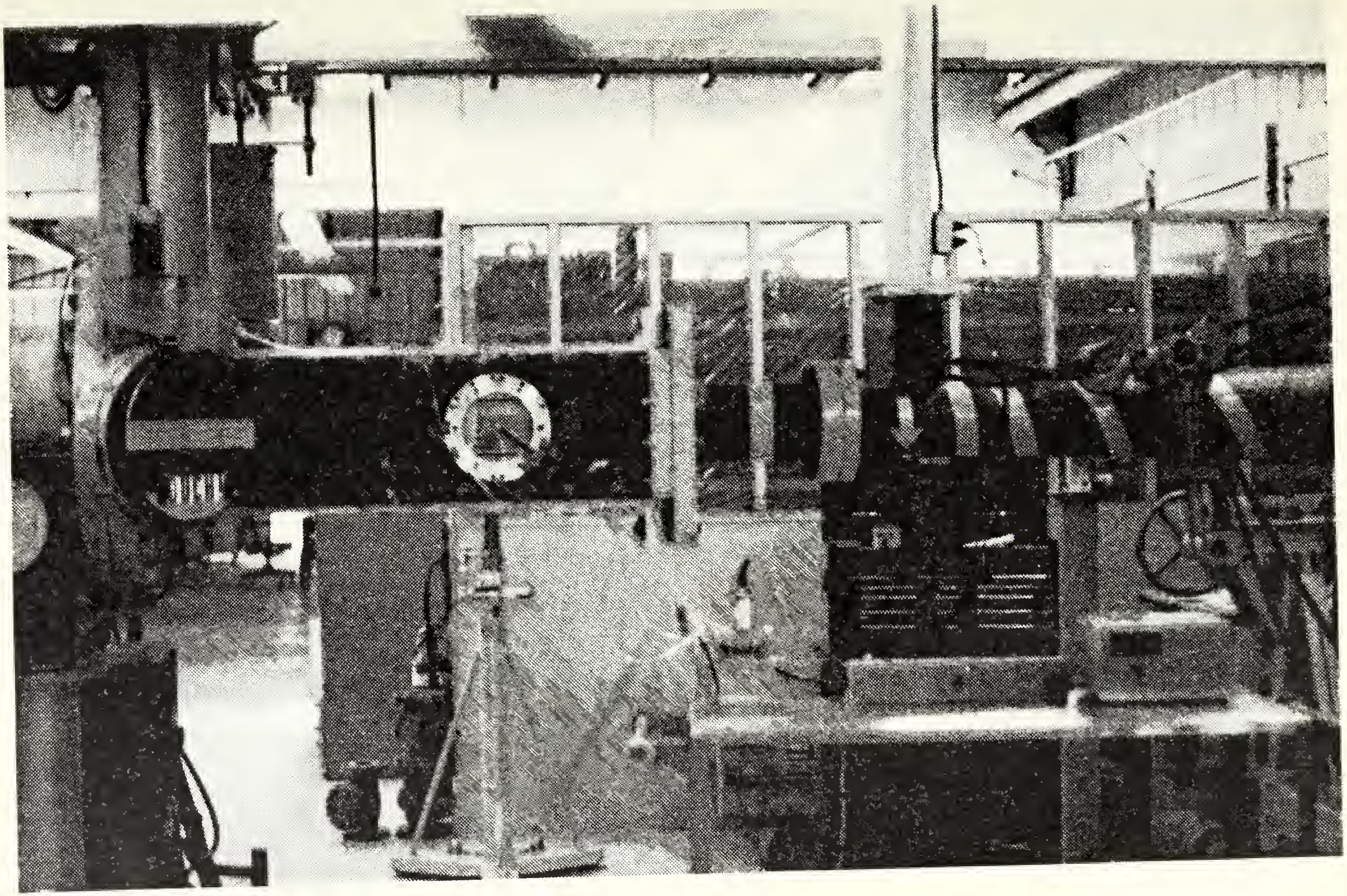

Figure 3-2 Naval Postgraduate School Supersonic Wind Tunnel and Associated Instrumentation (Front View)

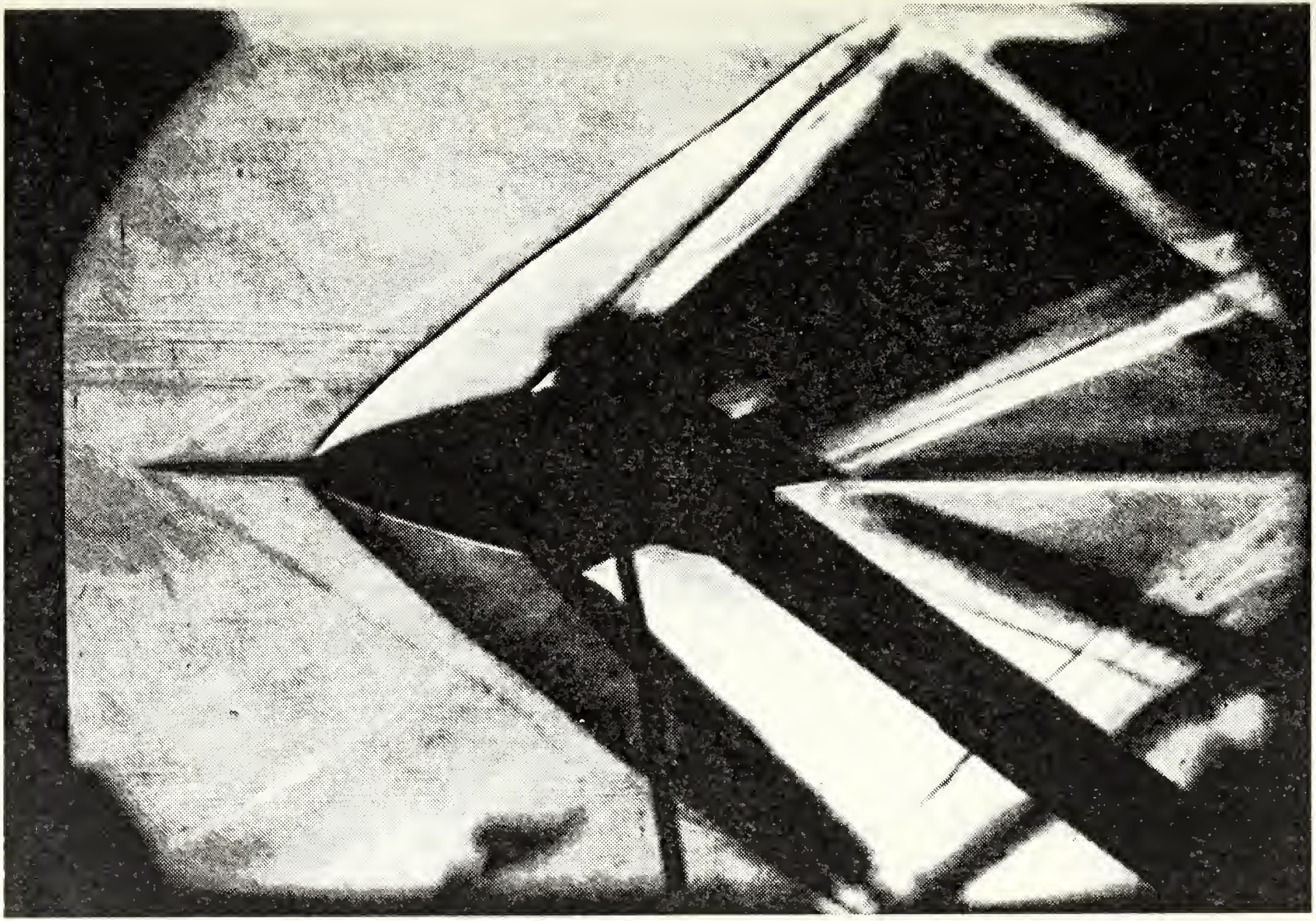

Figure 3-3 Schlieren Photograph of the Model Mounted in the Wind Tunnel;
α = *0 Degrees and* M_∞ = *1.92*

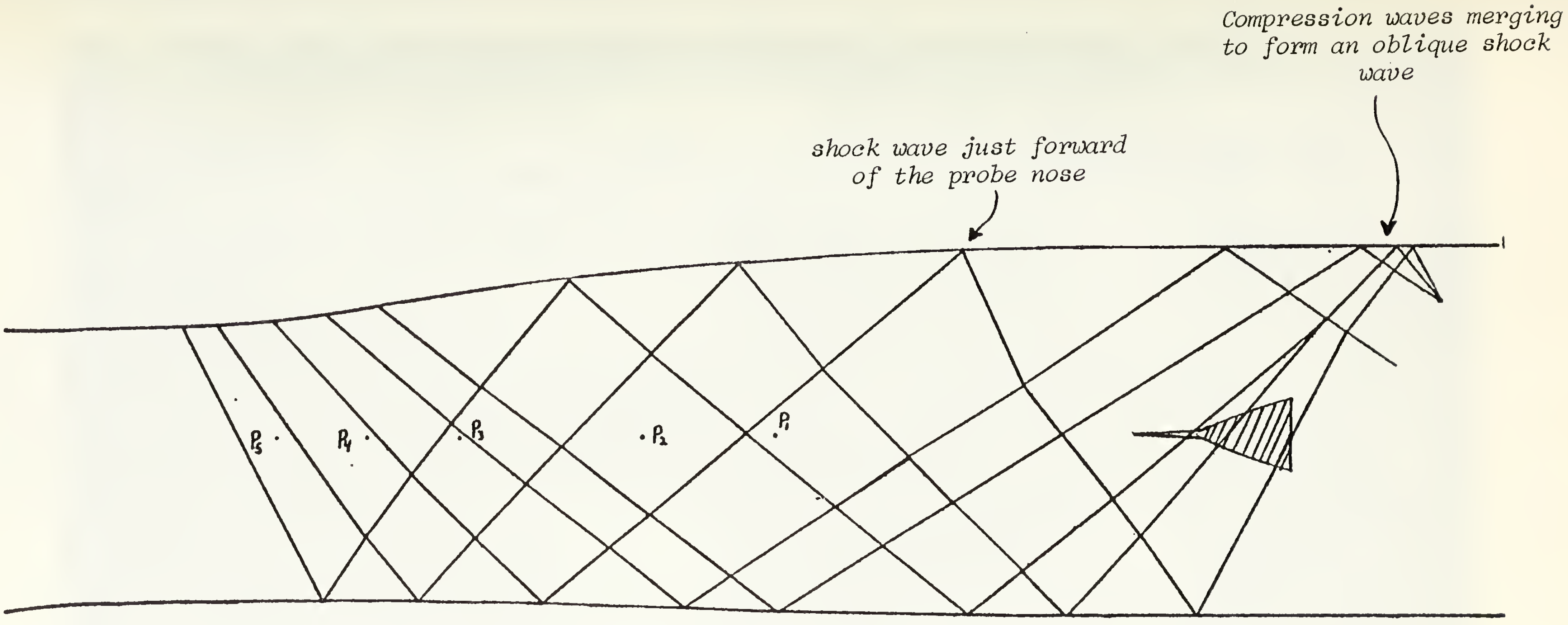
Compression waves merging to form an oblique shock wave
shock wave just forward of the probe nose
P1
P2
P3
P4
P5

Figure 3-4 Theoretical Mach Number Gradient and the Shock Waves in the Wind Tunnel Test Section That Result from Using the Combination of Mach 1.4 (Bottom) and 2.0 (Top) Nozzle Blocks

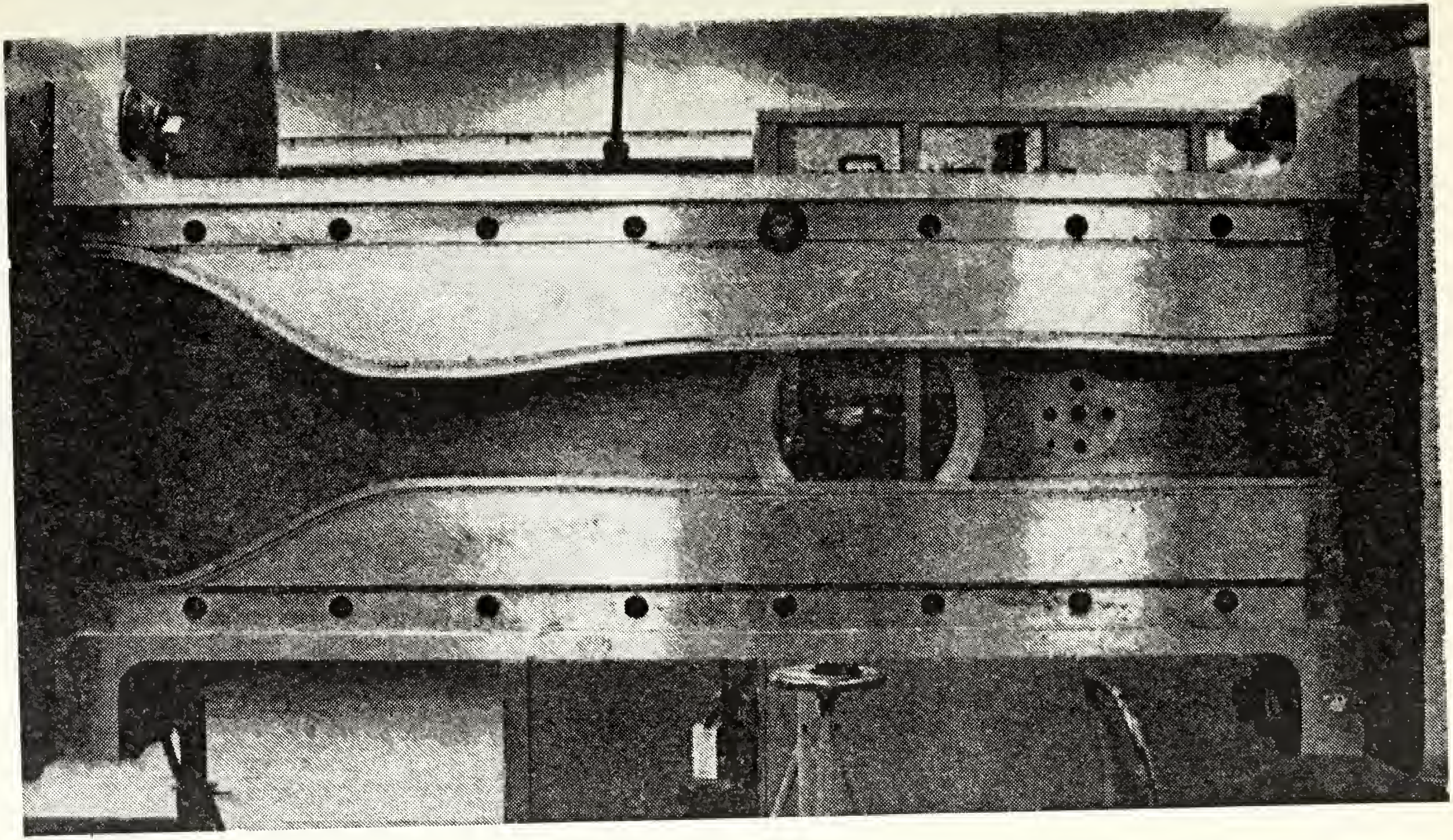

Figure 3-5 Photograph of the Mach 2.0 and Mach 1.4 Nozzle Blocks Installed in the Wind Tunnel (Mach 2.0 Block is the Upper Block)

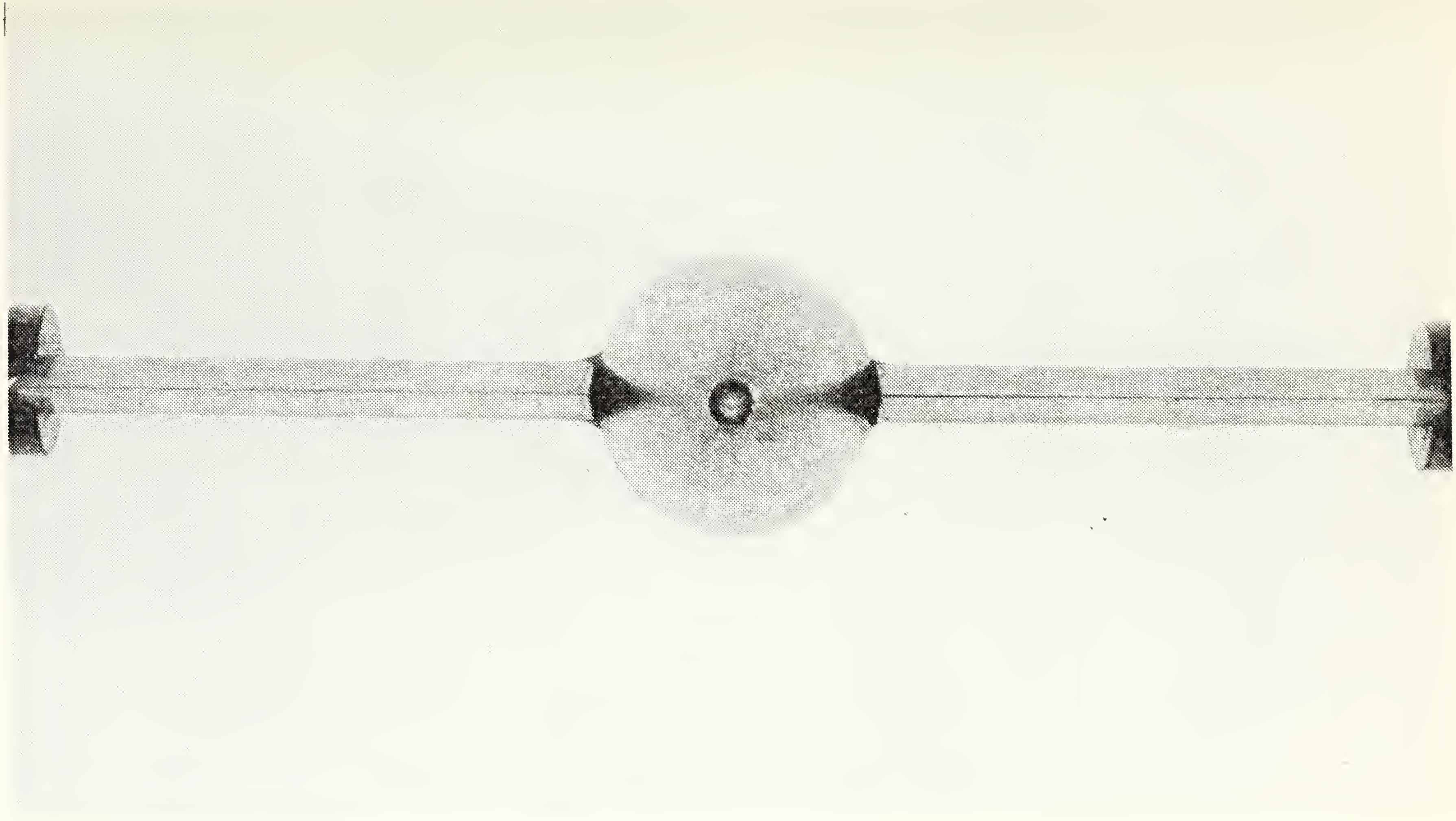

Figure 3-6 Front View of the Model and Double-Wedge Airfoil Used to Mount the Model in the Wind Tunnel

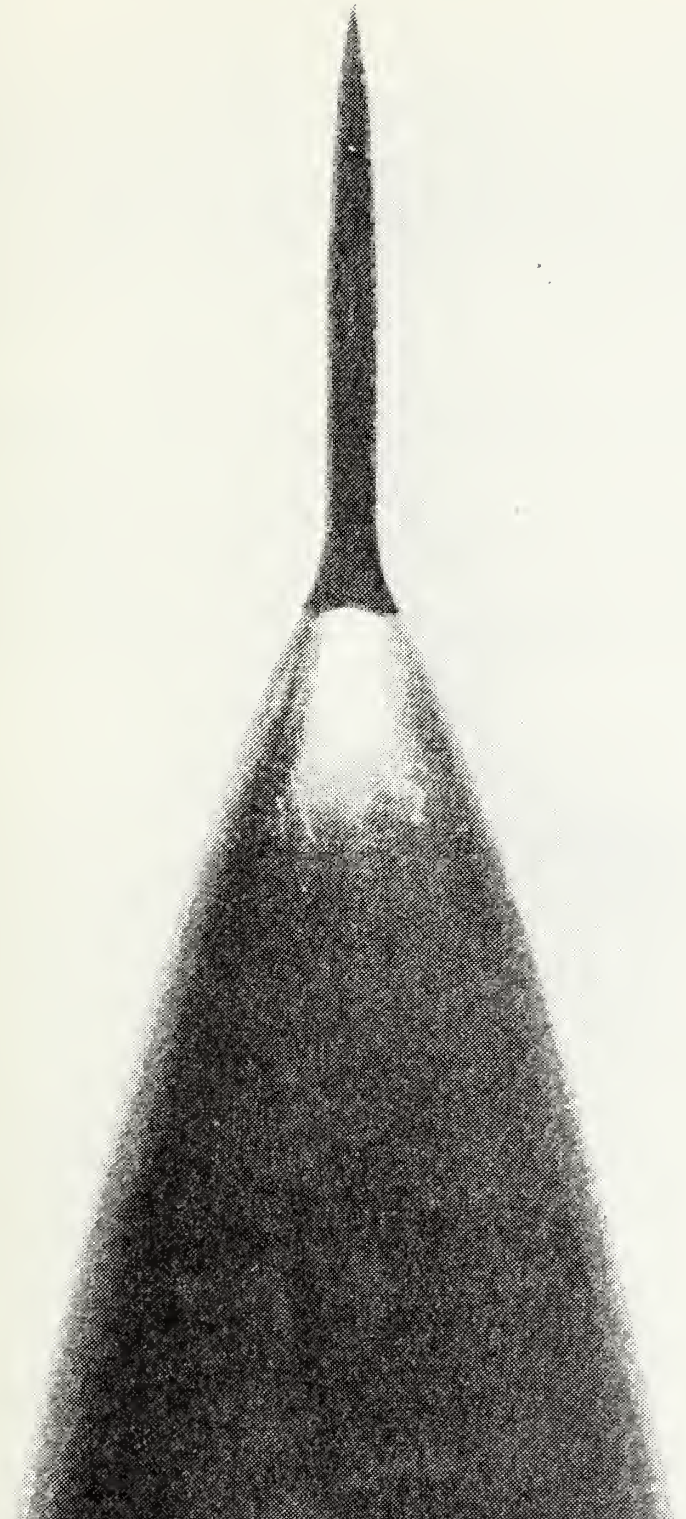

Figure 3-7 Photograph of the Model Ogive Nose and the Extended Static Pressure Probe

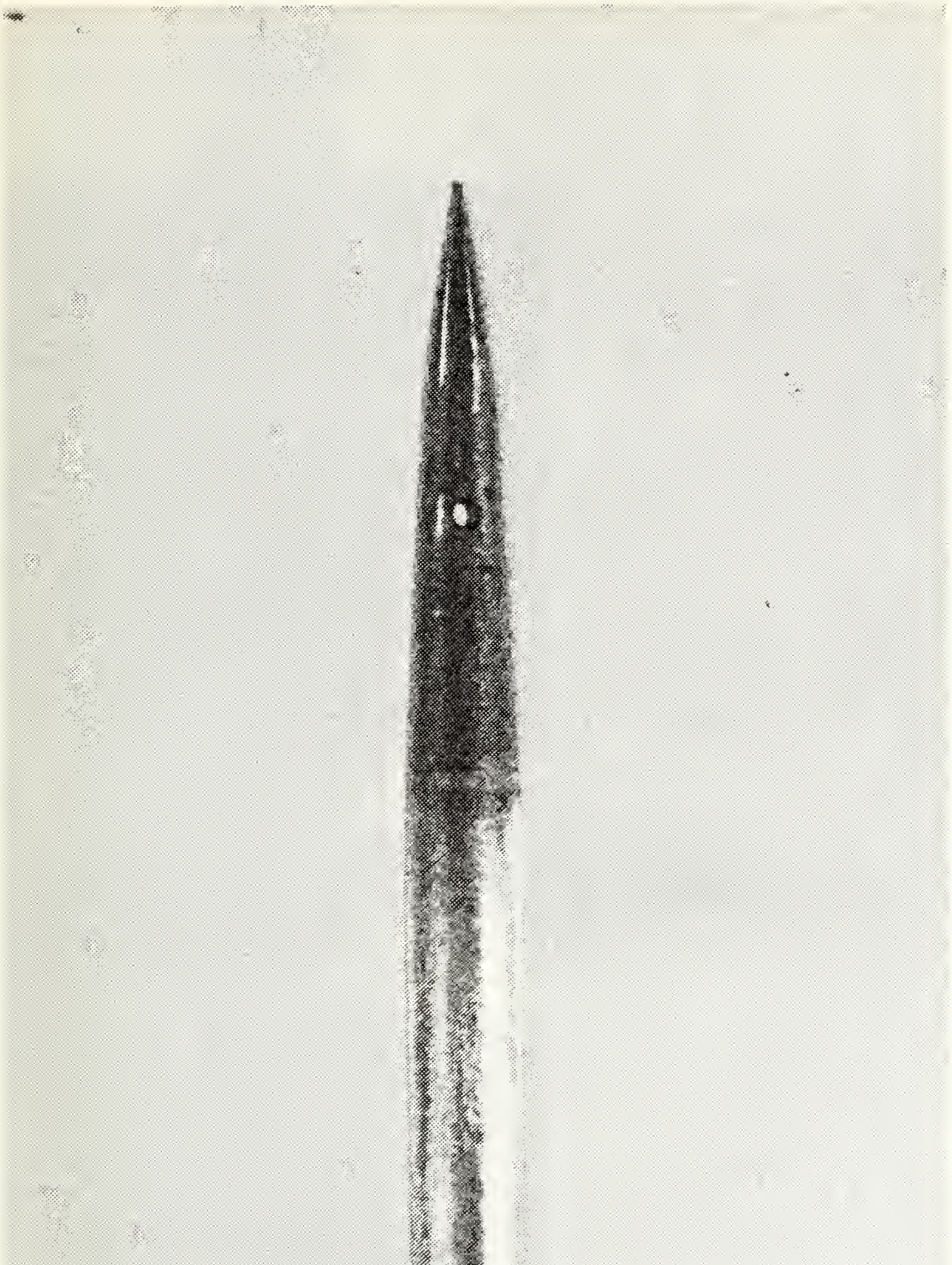

Figure 3-8 Photograph of the Static Pressure Probe Mated to the Missile Nose

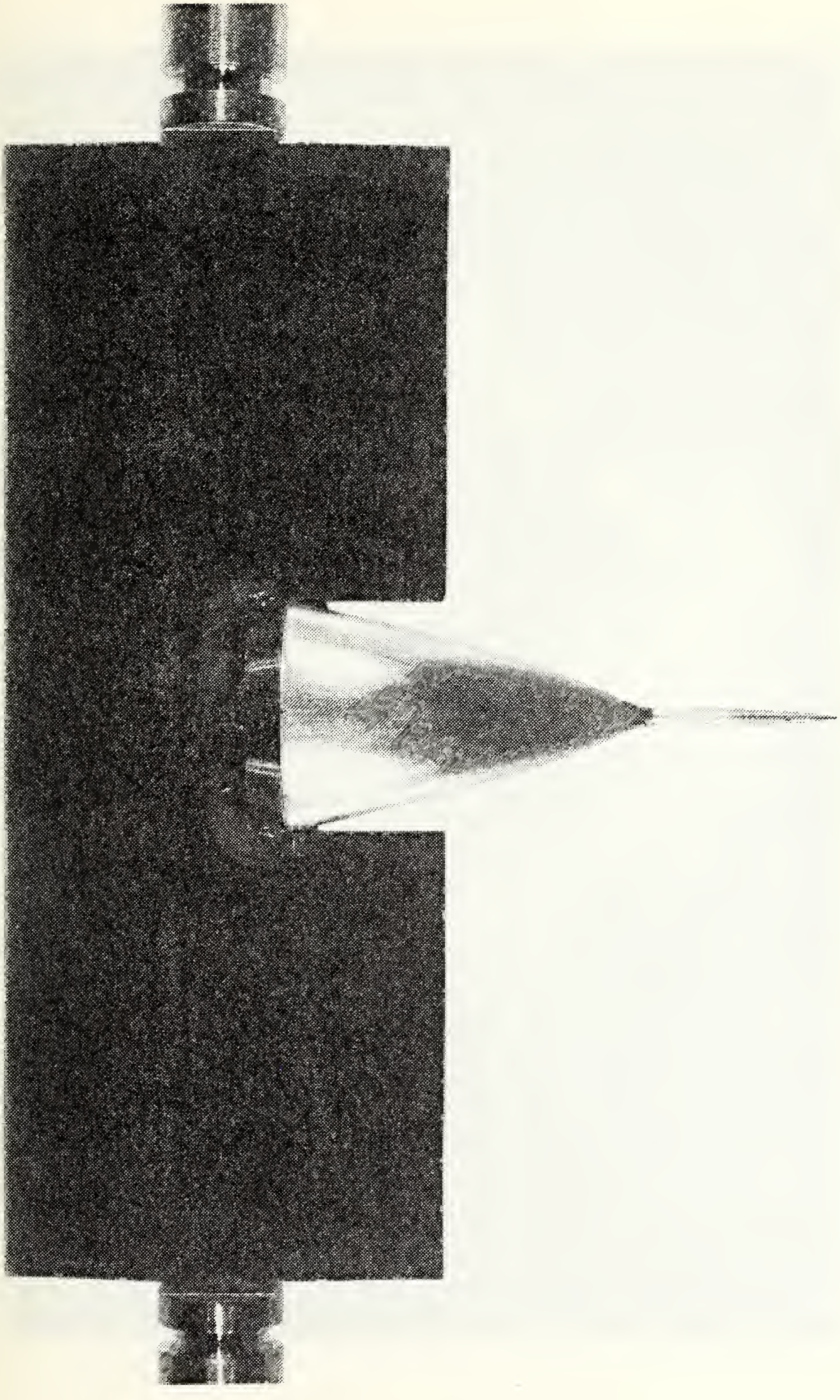

Figure 3-9 Top View of the Model and Mounting Wedge

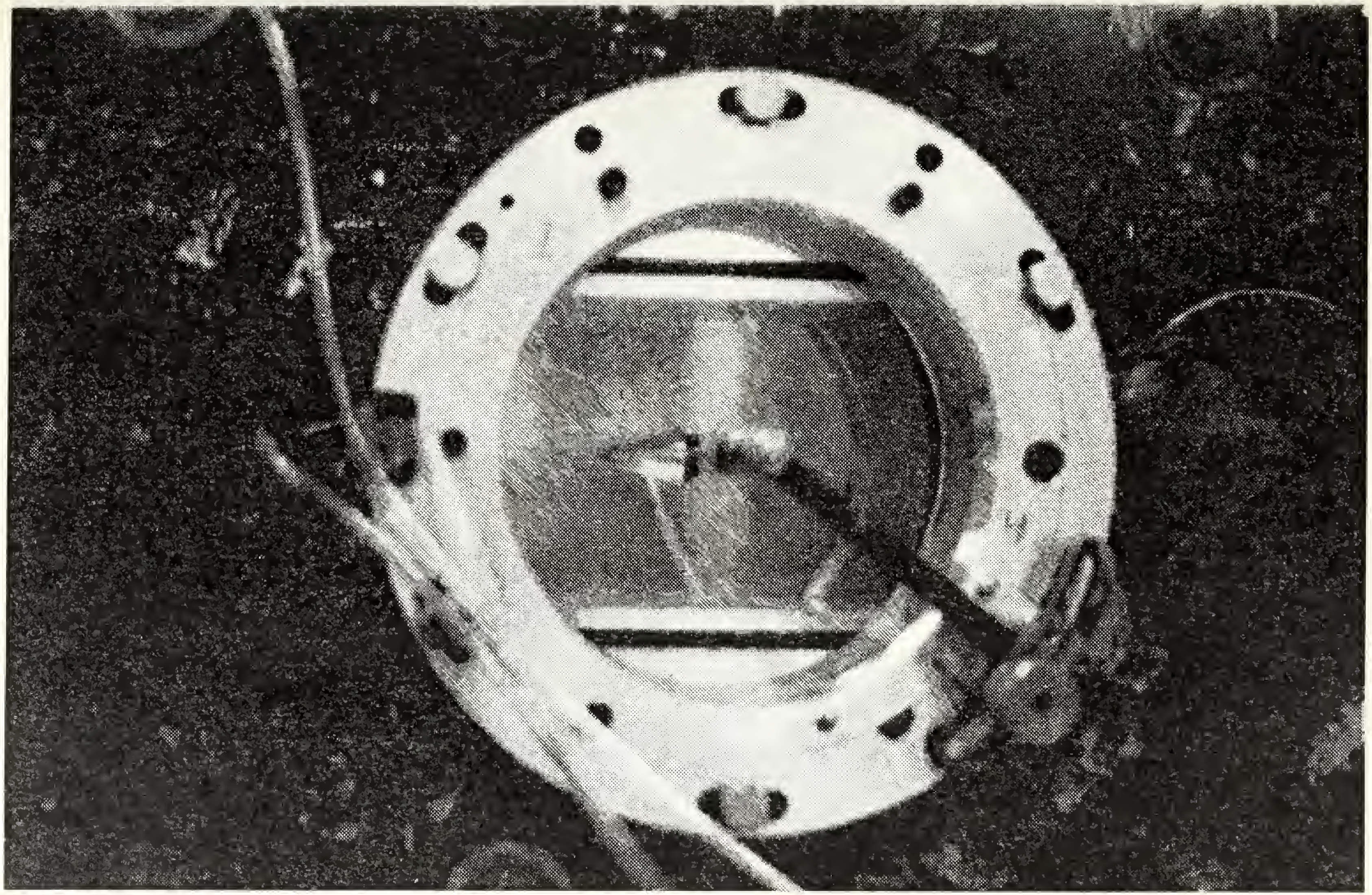

Figure 3-10 Photograph of the Model Mounted in the Wind Tunnel

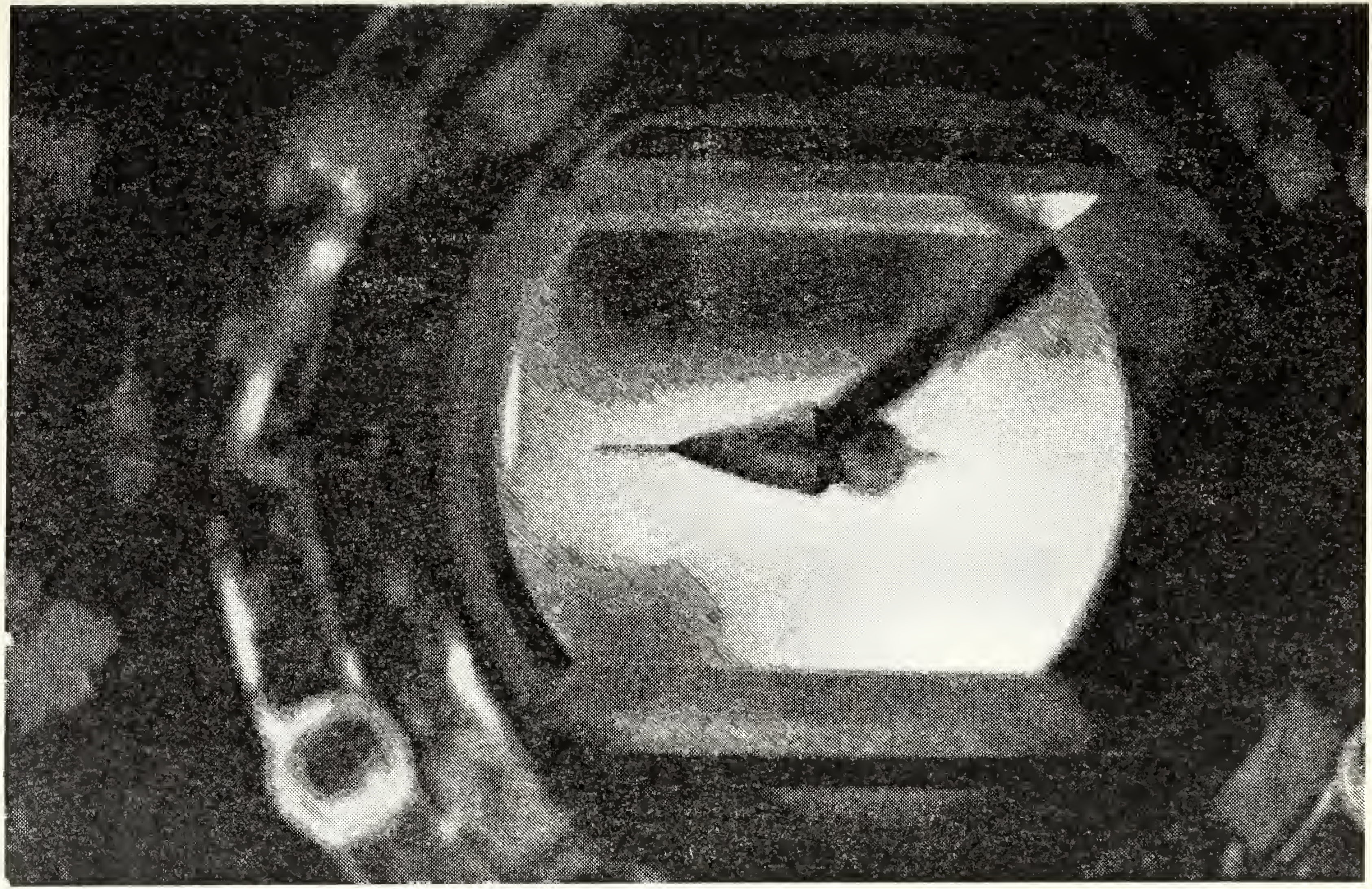

Figure 3-11 Close-Up View of the Model Mounted in the Wind Tunnel

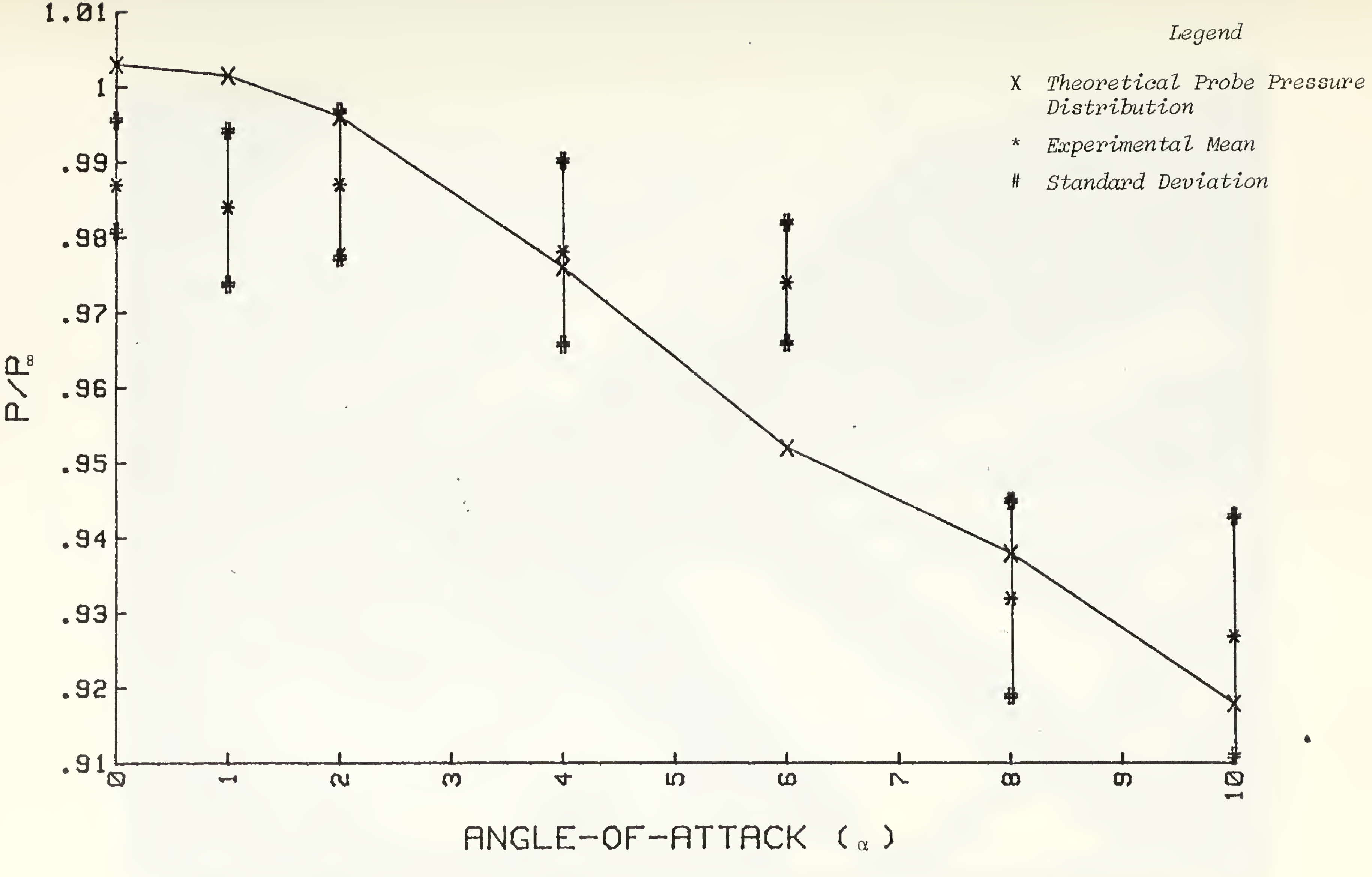

Figure 4-1 Plot of Experimental Results for $M_\infty = 1.92$: Angle-of-Attack Versus P/P_∞ and Probe Theoretical Performance

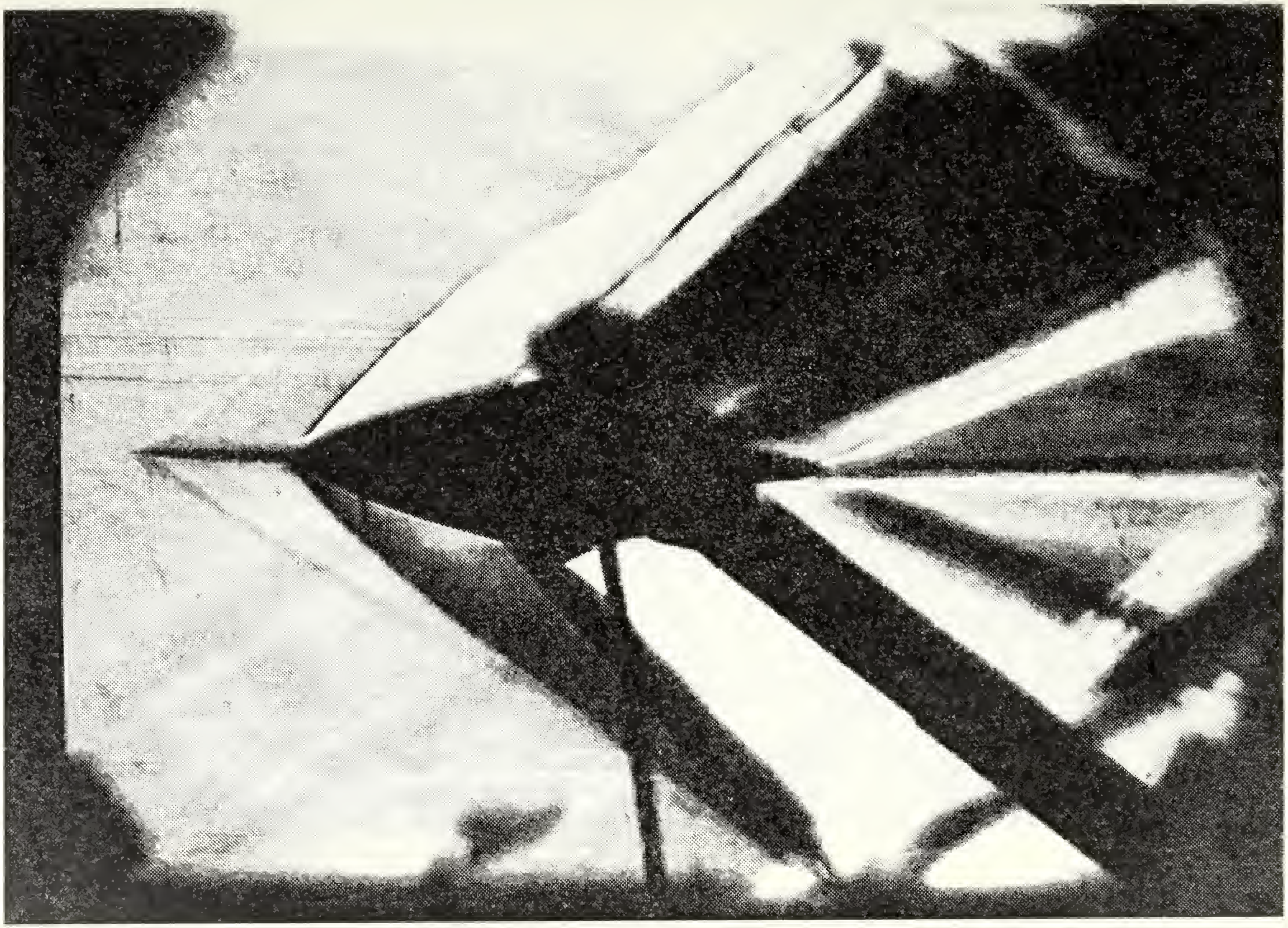

Figure 4-2 Schlieren Photograph of the Model Oriented at $\alpha = +1$ Degree In the Wind Tunnel Operating at $M_\infty = 1.92$

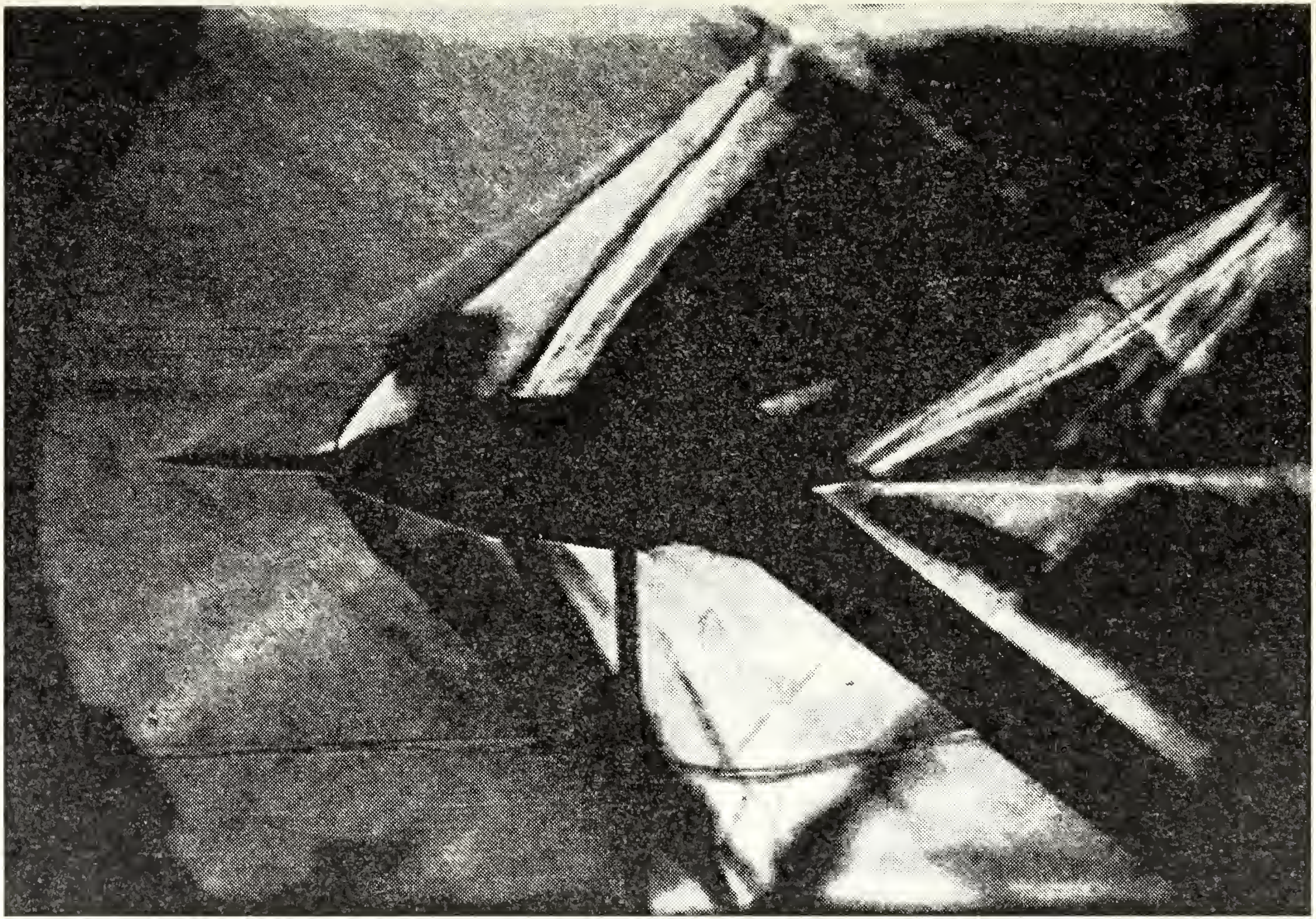

Figure 4-3 Schlieren Photograph of the Model in the Wind Tunnel Test Section:
$M_\infty = 1.51$ *and* $\alpha = 4$ *Degrees*

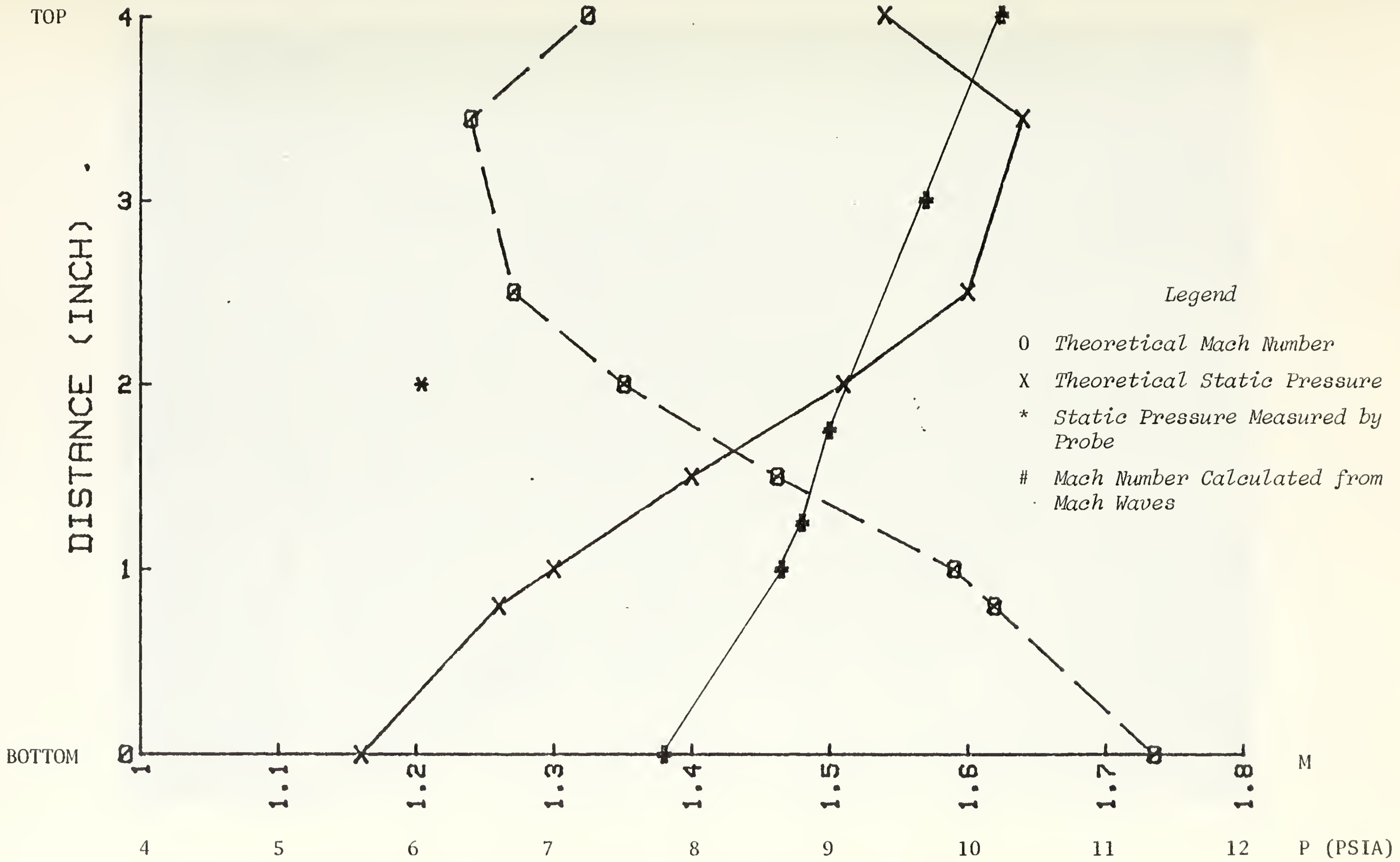

Figure 4-4 Graph of Distance Versus Theoretical Mach Number and Pressure (PSIA) in the Wind Tunnel Test Section

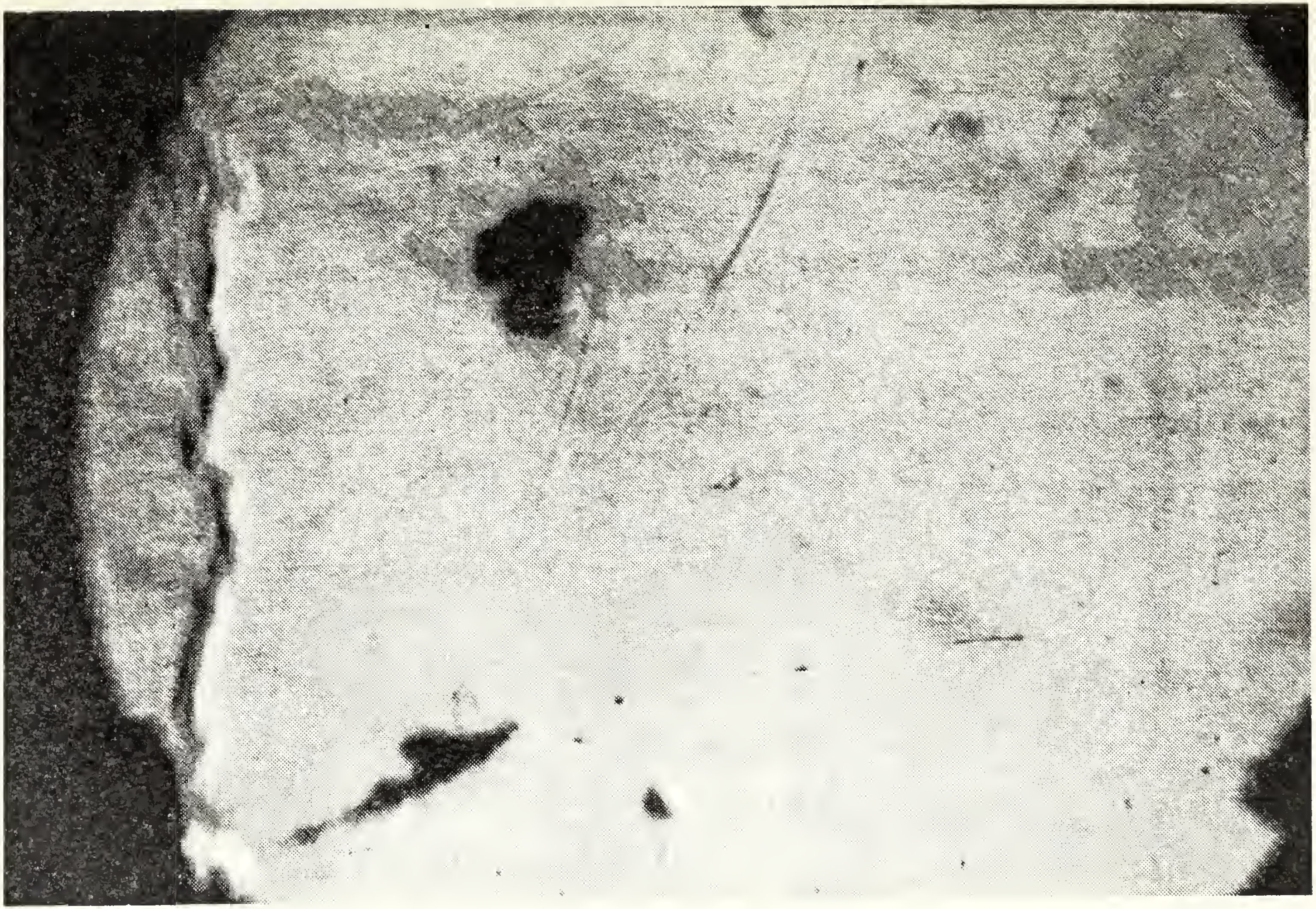

Figure A-1 Schlieren Photograph of Shock in Wind Tunnel Test Section During an Attempt to Obtain Supersonic Flow with the Mach 1.4 Nozzle Blocks

APPENDIX A: PRESSURE DISTRIBUTION PROGRAM LISTING AND SAMPLE DATA RUNS

Note: In this typed listing, and in the sample data runs, the character "°" signifies "greater than," and "±" signifies "less than." The ampersand (&) denotes exponentiation.

```
00001 LPRINT"SUPERSONIC FLOW PRESSURE COEFFICIENTS ABOUT A YAWED,"

00002 LPRINT"SLENDER, POINTED, BODY OF REVOLUTION. PROGRAM BY"

00003 LPRINT"J.R.SCHONBERGER AND K.D.TILLOTSON. BASED ON "

00004 LPRINT"CALCULATION PROCEDURES BY PROF. T.H.GAWAIN."

00005 LPRINT"NAVAL POSTGRADUATE SCHOOL, MONTEREY CA. FALL 1980"

00006 CLEAR

00010 CLS:PI=3.14159

00020 DIM A(20,20),B(20,20),C(20,20),CP(20),D(20,20),F F(20),G(20),GA(2
      0),GB(20),GC(20),GN(20),GO(20),GP(20),IX(20),JO(20),JR(20),JX(20
      ),R(20),RP(20),T(20,20),X(20),PR(20)

00025 LPRINT"ENTER X1";:INPUT X1:LPRINT X1

00027 LPRINT"ENTER X2";:INPUT X2:LPRINT X2

00029 LPRINT"ENTER X3";:INPUT X3:LPRINT X3

00031 LPRINT"ENTER B1";:INPUT B1:LPRINT B1

00033 LPRINT"ENTER B2";:INPUT B2:LPRINT B2

00035 LPRINT"ENTER COEFF A";:INPUT AA:LPRINT AA

00037 LPRINT"ENTER COEFF B";:INPUT BB:LPRINT BB

00039 LPRINT"ENTER COEFF C";:INPUT CC:LPRINT CC

00041 LPRINT"ENTER RX2";:INPUT RX:LPRINT RX

00043 LPRINT"ENTER FREE STREAM MACH NBR";:INPUT M:LPRINT M

00045 MU=ATN(1/M/SQR(-1/M*1/M+1))

00047 RY=RX+TAN(MU)*(X3-X2)

00049 LPRINT"ENTER NBR OF SUBINTERVALS";:INPUT N:LPRINT N:J=N-1

00051 LPRINT"ENTER LENGTH OF SUBINTERVAL";:INPUT H:LPRINT H
```

```
00053 FOR Z=1TOJ

00055 X(Z)=Z*H/(1-TAN(B1)/TAN(MU))

00057 R(Z)=X(Z)*TAN(B1)

00059 RP(Z)=TAN(B1)

00061 IF X(Z)±=X1 THEN NEXT Z ELSE 63

00063 FOR Y=ZTOJ

00065 R=1-AA/(TAN(MU))&2

00067 S=-1*(2*Y*H+BB/(TAN(MU))&2)

00069 T=-1*CC/(TAN(MU))&2+(Y*H)&2

00071 X(Y)=(-S+SQR(S&2-4*R*T))/(2*R)

00073 R(Y)=SQR(AA*X(Y)&2+BB*X(Y)+CC)

00075 RP(Y)=(2*AA*X(Y)+BB)/(2*R(Y))

00077 IF X(Y)±=X2 THEN NEXT Y ELSE 79

00079 FOR Z=YTOJ

00081 X(Z)=((RX-X2*TAN(B2))/TAN(MU)+Z*H)/(1-TAN(B2)/TAN(MU))

00083 R(Z)=TAN(B2)*X(Z)+RX-TAN(B2)*X2

00085 RP(Z)=TAN(B2)

00087 IF X(Z)±=X3 THEN NEXT Z ELSE 89

00089 FOR Y=ZTOJ

00091 X(Y)=RY/TAN(MU)+Y*H

00093 R(Y)=RY

00095 RP(Y)=0

00097 NEXT Y

00099 LPRINT TAB(1)"J";TAB(10)"X(J)";TAB(20)"R(J)";TAB(30)"RP(J)"

00101 FOR Z=1TOJ

00103 LPRINT TAB(1)Z;TAB(10)X(Z);TAB(20)R(Z);TAB(30)RP(Z)
```

```
00110 IF Z=10 THEN INPUT"PRESS ENTER TO CONTINUE";N$

00120 NEXT Z

00190 B=SQR(M&2-1)

00192 ON ERROR GOTO 1200

00195 U=0

00200 FOR Z=1TOJ

00205 U=U+1

00210 FOR Y=0TOU

00220 T(Z,Y)=SQR((X(Z)-Y*H)&2-(B*R(Z))&2)

00230 NEXT Y

00231 NEXT Z

00235 U=0

00240 FOR Z=1TOJ

00245 U=U+1

00250 FOR Y=1TOU

00260 A(Z,Y)=LOG(((X(Z)-(Y-1)*H)+T(Z,Y-1))/((X(Z)-Y*H)+T(Z,Y)))

00270 NEXT Y

00275 NEXT Z

00280 FOR Z=1TOJ

00290 FOR Y=1TOJ

00300 B(Z,Y)=(T(Z,Y-1)-T(Z,Y))/R(Z)

00310 NEXT Y

00311 NEXT Z

00320 FOR Z=1TOJ

00330 FOR Y=1TOJ

00340 C(Z,Y)=B(Z,Y)-RP(Z)*A(Z,Y)
```

```
00350 NEXT Y

00351 NEXT Z

00355 U=0

00360 FP(1)=RP(1)/C(1,1)

00370 FOR Z=2 TO J

00380 U=U+1

00390 FOR Y=1TOU

00400 W=W+C(Z,Y)*FP(Y)

00410 NEXT Y

00420 FP(Z)=(RP(Z)-W)/C(Z,Z)

00430 W=0

00440 NEXT Z

00450 FOR Z=1TOJ

00460 FOR Y=1TOJ

00470 W=W+A(Z,Y)*FP(Y)

00480 NEXT Y

00490 IX(Z)=W

00500 W=0

00510 NEXT Z

00520 FOR Z=1TOJ

00540 NEXT

00550 FOR Z=1TOJ

00560 GO(Z)=(1-(1+RP(Z)&2)*(1-IX(Z))&2+(M*IX(Z))&2)

00565 NEXT Z

00610 FOR Z=1 TO J

00620 FOR Y=1 TO Z
```

```
00630 D(Z,Y)=((X(Z)-(Y-1)*H)*T(Z,Y-1)-(X(Z)-Y*H)*T(Z,Y))/(2*R(Z)&2)
00640 NEXT Y
00650 NEXT Z
00660 FOR Z=1 TO J
00670 FOR Y=1 TO Z
00680 D(Z,Y)=-D(Z,Y)+B&2*A(Z,Y)+(X(Z)-(Y-1)*H)*B(Z,Y)/R(Z)
00690 NEXT Y
00700 NEXT Z
00710 FOR Z=1TOJ
00720 FOR Y=1TOZ
00730 D(Z,Y)=(D(Z,Y)+B&2*A(Z,Y)+RP(Z)*B(Z,Y))
00740 NEXT Y
00750 NEXT Z
00760 G(0)=0:GP(1)=1/D(1,1):U=0
00770 FOR Z=2TOJ
00780 W=0:V=0
00790 U=U+GP(Z-1)
00800 G(Z-1)=H*U
00810 FOR Y=1TOZ
00820 W=W+D(Z,Y-1)*GP(Y-1)
00830 V=V+B(Z,Y)*G(Y-1)
00840 NEXT Y
00850 GP(Z)=(1-V/R(Z)-W)/D(Z,Z)
00860 NEXT Z
00870 FOR Z=1TOJ
00880 U=0:V=0
```

```
00890 FOR Y=1TOZ

00900 U=U+B(Z,Y)*GP(Y)

00910 V=V+A(Z,Y)*GP(Y)

00920 NEXT Y

00930 JX(Z)=U

00940 JR(Z)=V*B&2

00950 JO(Z)=1-JR(Z)-RP(Z)*JX(Z)

00970 NEXT Z

00990 FOR Z=1TOJ

01010 GN(Z)=((1+RP(Z)&2)*(1-IX(Z))+M&2*IX(Z))*JX(Z)

01020 GA(Z)=-1*M&2*IX(Z)&2+(1+RP(Z)&2)*(1-IX(Z))&2

01030 GB(Z)=(M&2-1-RP(Z)&2)*JX(Z)&2

01040 GC(Z)=(1+JO(Z))&2

01050 NEXT Z

01055 CLS

01060 LPRINT"ENTER THE ANGLE OF ATTACK A (IN RADIANS)";:INPUT A:LPRINT
       A

01070 LPRINT"ENTER THE RADIAL ANGLE THETA (IN RADIANS)";:INPUT T:LPRIN
      T T

01071 LPRINT"ENTER TEMP (KELVIN)";:INPUT TE:LPRINT TE

01072 LPRINT"ENTER PRESSURE (N/M&2)";:INPUT PE:LPRINT PE

01073 LPRINT"ENTER DENSITY (KG/M&3)";:INPUT PO:LPRINT PO

01080 FOR Z=1TOJ

01090 CP(Z)=GO(Z)-2*GN(Z)*SIN(A)*COS(A)*COS(T)+(GA(Z)+GB(Z)*(COS(T))&2
      -GC(Z)*(SIN(T))&2)*(SIN(A))&2

01095 PR(Z)=1+200.941*PO*TE*M&2*CP(Z)/PE

01100 NEXT Z
```

```
01120 LPRINTTAB(1)"J";TAB(10)"X(J)";TAB(20)"CP(X)";TAB(32)"PRESSURE RA
      TIO"

01130 FOR Z=1TOJ

01140 LPRINTTAB(1)Z;TAB(10)X(Z);TAB(20)CP(Z);TAB(32)PR(Z)

01160 NEXT Z

01170 LPRINT"IF YOU DESIRE TO CHANGE A AND THETA ENTER Y ELSE N";:INPU
      T N$:LPRINT N$

01180 IF N$="N" THEN END ELSE GOTO1055

01200 X(Z)=X(Z)+X(Z)*.001

01210 RESUME
```

Sample Data Run for Mach 2.0 at Angle of Attack $\alpha = 0$ and 10 Degrees

```
SUPERSONIC FLOW PRESSURE COEFFICIENTS ABOUT A YAWED,
SLENDER, POINTED, BODY OF REVOLUTION. PROGRAM BY
J.R.SCHONBERGER AND K.D.TILLOTSON. BASED ON
CALCULATION PROCEDURES BY PROF. T.H.GAWAIN.
NAVAL POSTGRADUATE SCHOOL, MONTEREY CA. FALL 1980
ENTER X1 100
ENTER X2 260
ENTER X3 400
ENTER B1 .17453
ENTER B2 .0523599
ENTER COEFF A-9.26731E-03
ENTER COEFF B 8.36762
ENTER COEFF C-402.881
ENTER RX2 33.856
ENTER FREE STREAM MACH NBR 2
ENTER NBR OF SUBINTERVALS 20
ENTER LENGTH OF SUBINTERVAL 15
 J        X(J)       R(J)       RP(J)
  1        21.5952    3.80776    .176324
  2        43.1905    7.61551    .176324
  3        64.7857    11.4233    .176324
  4        86.3809    15.231     .176324
  5        109.828    20.1081    .157449
  6        129.756    22.9529    .129889
  7        148.696    25.2279    .111218
  8        166.989    27.1293    .0971743
  9        184.81     28.7579    .0859282
  10       202.262    30.1736    .0765366
  11       219.414    31.4156    .0684513
  12       236.311    32.511     .0613283
  13       252.989    33.4798    .0549372
  14       269.503    34.354     .0524078
  15       286        35.2186    .0524078
  16       302.498    36.0832    .0524078
  17       318.996    36.9478    .0524078
  18       335.493    37.8124    .0524078
  19       351.991    38.677     .0524078
ENTER THE ANGLE OF ATTACK A (IN RADIANS) 0
ENTER THE RADIAL ANGLE THETA (IN RADIANS) 0
ENTER TEMP (KELVIN) 288.15
ENTER PRESSURE (N/M&2) 101325
ENTER DENSITY (KG/M&3) 1.225
```

```
 J        X(J)      CP(X)        PRESSURE RATIO
  1        21.5952   .114208      1.31979
  2        43.1905   .114208      1.31979
  3        64.7857   .114208      1.31979
  4        86.3809   .114208      1.31979
  5        109.938   .0989367     1.27703
  6        129.756   .0651711     1.18248
  7        148.696   .0455148     1.12744
  8        167.156   .0324173     1.09077
  9        184.81    .0229932     1.06438
  10       202.464   .015794      1.04422
  11       219.414   .0100775     1.02822
  12       236.311   5.30874E-03  1.01486
  13       252.989   1.29649E-03  1.00363
  14       269.503   1.17926E-03  1.0033
  15       286       3.38801E-03  1.00949
  16       302.498   5.17499E-03  1.01449
  17       318.996   6.62418E-03  1.01855
  18       335.493   7.80804E-03  1.02186
  19       352.343   8.76572E-03  1.02454
IF YOU DESIRE TO CHANGE A AND THETA ENTER Y ELSE NY
ENTER THE ANGLE OF ATTACK A (IN RADIANS) .0349
ENTER THE RADIAL ANGLE THETA (IN RADIANS) 3.1416
ENTER TEMP (KELVIN) 288.15
ENTER PRESSURE (N/M&2) 101325
ENTER DENSITY (KG/M&3) 1.225
 J        X(J)      CP(X)        PRESSURE RATIO
  1        21.5952   .132234      1.37026
  2        43.1905   .132234      1.37026
  3        64.7857   .132234      1.37026
  4        86.3809   .132234      1.37026
  5        109.938   .117314      1.32849
  6        129.756   .0821772     1.2301
  7        148.696   .0616945     1.17275
  8        167.156   .0482622     1.13514
  9        184.81    .0377925     1.10582
  10       202.464   .0303393     1.08495
  11       219.414   .0236319     1.06617
  12       236.311   .018247      1.05109
  13       252.989   .0136563     1.03824
  14       269.503   .0130074     1.03642
  15       286       .0147623     1.04134
  16       302.498   .0161278     1.04516
  17       318.996   .0171903     1.04813
  18       335.493   .0180226     1.05046
  19       352.343   .0190157     1.05325
IF YOU DESIRE TO CHANGE A AND THETA ENTER Y ELSE NN
```

APPENDIX B: COMPUTER PROGRAM AND SAMPLE DATA RUN FOR CALCULATING PROBE PLENUM PRESSURE

Program

```
00010 CLS

00020 INPUT "ENTER P1";P1

00030 INPUT "ENTER P2";P2

00040 INPUT "ENTER P3";P3

00050 PRINT "T=";T,"PP=";PP,"CASE=";CA

00060 INPUT "ENTER YOUR GUESS FOR PP";PP

00070 A=P1-PP

00080 B=P2-PP

00090 C=P3-PP

00100 IF B<=0 AND C<=0 THEN 200                                  (Case 3)

00110 IF C<=0 THEN 300                                           (Case 2)

00120 IF B<=0 THEN 400                                           (Case 1)

00130 PRINT"SOMETHING WRONG";:STOP

00200 T=SQR(2*ABS(A))-2*SQR(2*ABS(B))-SQR(2*ABS(C))

00210 CA=3

00220 GOTO 50

00300 T=SQR(2*ABS(A))+2*SQR(2*ABS(B))-SQR(2*ABS(C))

00310 CA=2

00320 GOTO 50

00400 T=SQR(2*ABS(A))-2*SQR(2*ABS(B))+SQR(2*ABS(C))

00410 CA=1

00420 GOTO 50
```

Sample Data Run (Reproduced from CRT display)

```
ENTER P1 ?1.019237
ENTER P2 ?.96525
ENTER P3 ?.964412
T= 0    PP= 0    CASE= 0
ENTER YOUR GUESS FOR PP ?.977
T= .174618    PP= .977    CASE= 3
ENTER YOUR GUESS FOR PP ?.970
T= .0131546    PP= .970    CASE= 3
ENTER YOUR GUESS FOR PP ?.971
T=-.0186603    PP= .971    CASE= 3
ENTER YOUR GUESS FOR PP ?.9705
T=-3.07509E-03    PP= .9705    CASE= 3
ENTER YOUR GUESS FOR PP ?.9704
T= 1.14933E-04    PP= .9704    CASE= 3
ENTER YOUR GUESS FOR PP ?.970404
T=-1.11237E-05    PP= .970404    CASE= 3
```

APPENDIX C: SEQUENTIAL LISTING OF TESTING

As stated in Chapter 3, Appendix C is a sequential listing of testing and corrective action taken between testing attempts, and a discussion of the three most likely reasons for the failure of the wind tunnel to start at Mach 1.4. Testing attempts, and the corrective actions taken between testing attempts, were as follows:

(1) Test Number One was conducted with the Mach 1.4 nozzle blocks installed and the model mounted in the wind tunnel test section. Supersonic flow could not be established in the test section. Test section blockage was considered to be the most probable cause. A higher percentage, 28%, of test section blockage is allowed at Mach 2; therefore, the decision was made to complete Mach 2 testing prior to reducing model and mounting system frontal area. The Mach 1.4 nozzle blocks were removed. The wind tunnel plenum chamber screen was discovered to be torn, and was hanging loose in the plenum chamber. The two functions of the screen are: (a) to obtain a flat velocity profile (flat stagnation pressure profile), and (b) to generate small-scale turbulence which dissipates prior to arrival at the test section. Sufficient manpower to replace the plenum chamber screen was not available. Therefore, the screen was removed.

(2) The Mach 2.0 nozzle blocks were installed. To insure that the flow in the wind tunnel test section was uniform, an additional pressure tap was installed in the wind tunnel wall opposite one of the existing pressure taps. Testing showed no significant pressure difference (approximately 0.5 percent) between the two pressure taps. Therefore, the test

section velocity profile was inferred to be reasonably uniform. Twenty-three Mach 2.0 wind tunnel tests were conducted with supersonic flow achieved in the test section (25 to 30 PSIG plenum chamber pressure).

(3) The Mach 2.0 nozzle blocks were removed, and the Mach 1.4 nozzle blocks were reinstalled. The model was mounted in the wind tunnel, and testing was attempted. Supersonic flow in the test section was not achieved.

(4) The model frontal area was reduced by 14 percent (yielding 5.4 percent test section blockage) by machining 0.050 inch from the top and bottom of the missile nose ogive. Supersonic flow still could not be achieved.

(5) Model frontal area then was reduced by an additional 30 percent (yielding 3.5 percent test section blockage) by machining an additional 0.060 inch from the top and bottom of the missile nose ogive and 0.015 inch from the top and bottom of the double edge airfoil. After the reduction in blockage, supersonic flow could not be achieved.

(6) Four boundary-layer bleed valves were installed in both wind tunnel walls, just forward of the nozzle second throat, to decrease the required mass flow rate through the second throat. A complete description of the bleed valve specifications and function can be found in Habel [8]. Once again, supersonic flow could not be achieved.

(7) The bleed valves and the model were removed from the wind tunnel. Attempts to obtain supersonic flow in the wind tunnel test section failed with no wind tunnel blockage.

(8) A fine-mesh screen was installed in the wind tunnel just forward of the nozzle first throat. With the screen, but without the model,

supersonic flow could not be achieved. Figure A-1 is a photograph of the shock that was observed in the wind tunnel test section between 25 and 65 PSIG plenum chamber pressure.

The three most probable causes of the failure to obtain supersonic flow were: (a) that the model was too large, resulting in choked flow; (b) that the wind tunnel plenum chamber screen was missing, causing an uneven velocity profile; and (c) that the Mach 1.4 nozzle block second throat was too small, resulting in choked flow. These factors, of course, can operate in combination as well as singly.

Model size was ruled out as a cause of failure due to two considerations. First, after reduction of the model's frontal area, the actual wind tunnel blockage, 3.5 percent, was well below the 6.4 percent theoretical allowed wind tunnel blockage. Second, supersonic flow could not be achieved even without the model in the wind tunnel. The wind tunnel plenum chamber screen and the nozzle block second throat, however, remained as probable causes of testing failure.

The inside dimensions of the Mach 1.4 nozzle blocks were measured, and the areas of the first and second throats were 14.36 and 15.61 square inches, respectively. The ratio of second throat area to first throat area was thus 1.09. Using the calculation method presented in Liepman and Roshko [6], the theoretical minimum area ratio allowable is 1.04. Therefore, the Mach 1.4 nozzle block design allows a safety factor of approximately five percent for the boundary layer in the second throat.

Since there is less constriction in the Mach 1.4 nozzle than in the Mach 2.0 nozzle, an uneven velocity profile would affect more adversely the flow in the Mach 1.4 nozzle. The adverse effect of the uneven velocity

profile may have enlarged the boundary layer in the second throat, thus preventing supersonic flow.

LIST OF REFERENCES

1. Pinckney, S. Z., *A Short Static-Pressure Probe Design for Supersonic Flow*, National Aeronautics and Space Administration, NASA TN D-7978, July 1975

2. Kuethe, A. M., and Chow, C., *Foundations of Aerodynamics: Basis of Aerodynamic Design*, Third Edition, Wiley, 1976

3. Gawain, T. H., and Schonberger, J. R., *Linearized Supersonic Flow About a Body of Revolution with Corrected Boundary Conditions*, Naval Postgraduate School Technical Report, NPS 67-80-010, September 1980

4. *U. S. Standard Atmosphere, 1976*, National Oceanic and Atmospheric Administration, National Aeronautics and Space Administration, United States Air Force

5. Streeter, V. L., and Wylie, E. B., *Fluid Mechanics*, Seventh Edition, McGraw-Hill, 1979

6. Liepmann, A. H., and Roshko, A., *Elements of Gas Dynamics*, Wiley, 1957

7. Haber, A., and Runyon, R., *General Statistics*, Addison-Wesley, 1973

8. Habel, P. G., *A Study of Boundary Layer and Mass Bleed in a Short Length Supersonic Diffuser for a Gas Dynamic Laser*, Master's Thesis, Naval Postgraduate School, March 1976

INITIAL DISTRIBUTION LIST

		No. Copies
1.	Defense Technical Information Center Cameron Station Alexandria, Virginia 22314	2
2.	Library, Code 0142 Naval Postgraduate School Monterey, California 93940	2
3.	Department Chairman, Code 67 Department of Aeronautics Naval Postgraduate School Monterey, California 93940	1
4.	Professor Allen E. Fuhs, Code 67Fu Department of Aeronautics Naval Postgraduate School Monterey, California 93940	10
5.	Professor T. H. Gawain, Code 67Gn Department of Aeronautics Naval Postgraduate School Monterey, California 93940	2
6.	Mr. Ronald Dettling Naval Weapons Center China Lake, California 93555	9
7.	LCDR K. D. Tillotson, USN 15714 58th Place West Edmonds, Washington 98020	3
8.	Lt. J. R. Schonberger, USN 1920 Catherine Drive Bismarck, North Dakota 58501	1
9.	LCDR P. G. Habel, USN 234 Tryon Middleton, Connecticut 06457	1
10.	Captain G. M. Harding, USAR P.O. Box 7556 Carmel, California 93921	1
11.	Mr. S. Z. Pinckney Langley Research Center Hampton, Virginia 23665	1

Thesis
T485
c.1
Tillotson
191166
Analysis and wind tunnel tests of a static pressure probe used to sense altitude through measurement of static pressure.

24 JUL 90
36026

Thesis
T485
c.1
Tillotson
191166
Analysis and wind tunnel tests of a static pressure probe used to sense altitude through measurement of static pressure.

thesT485
Analysis and wind tunnel tests of a stat
3 2768 002 03534 7
DUDLEY KNOX LIBRARY